EPFL: Swiss Federal Institute of Technology in Lausanne
ENAC: School of Architecture, Civil & Environmental Engineering
IIC: Civil Engineering Institute
MCS: Structural Maintenance and Safety Laboratory

Master's Project Fall 2021/2022

Nizar Jaber

Structural Response of ''La Jument'' Lighthouse under Extreme Wave Loading – Analysis and Concept of Maintenance

Supervisor: Dr. Emmanuel Denarié, MER, EPFL

January 2022

{The page is left blank intentionally}

Preface

This research was completed in Fall semester 2021-2022 in the Structural Maintenance and Safety Laboratory and corresponds to 17 weeks of work and 30 credits. The four months' work period demanded discipline and hard work but provided an irreplaceable learning experience.

The research was conducted under the supervision of MER DR. Emmanuel Denarié in collaboration with CEREMA/Brest, Nicolas Fady. Their professional advice and input have been extremely educational and have greatly contributed to an increased understanding of all aspects of this project as well as provided me with the engineering sense to reach satisfactory results.

I express my sincere appreciation and gratitude to my supervisor for his valuable suggestions, guidance, encouragements, and insight throughout the study.

I would like to offer my special thanks to Mr. Nicolas Fady from CEREMA/ Brest for his constructive critics and involvement during many motivating discussions that guided me throughout the research process. I would like to thank Mr. Xavier Kergadallan (CEREMA/Brest) for his support on wave loadings and Professor Alan O'Connor from Trinity College Dublin for accepting to review this project as an external expert.

I would further like to convey my gratitude to my family and friends for their continuous and unconditional support to accomplish a thesis that meets my desires.

Nizar Jaber
Lausanne, January 2022

{The page is left blank intentionally}

Abstract

Ancient off-shore lighthouses have a phenomenal cultural significance. They were built as physical aid for navigation to guide mariners and to warn them from dangerous shallow rocky reefs. Understanding their structural response under waves loading is a challenging task.

La Jument lighthouse, off the coast of Brittany, has sustained extreme environmental loading for more than 110 years. The main motivation of the present study is to characterize its structural response under extreme waves loading by 3D Finite Element Modeling using the commercial software DIANA. The model is calibrated based on the data collected from accelerometers and photographical documentations during a measurement campaign in winter 2018 in which the highest wave recorded with 19 meters height is considered for this study. The effect on the lighthouse's structural response of slamming pressure magnitude, tide level, and slamming area is investigated in a parametric study.

The predictions of the FE model were comparable to the actual measurements confirming the main hypothesis in this study. The tide level was proven to be an important factor contributing to the structural response parameters. The FE model suggested 230 kPa as the most likely pressure of the wave under consideration.

Moreover, intervention methods using UHPFRC combined with a measurement campaign are proposed to preserve the outstanding cultural significance of La Jument lighthouse. Extending the life of off-shore lighthouses is essential to understand non-linear characteristics of extreme waves in future field measurements which helps validating numerical computations and removing uncertainties about their dynamic behavior.

Key Words

Off-shore lighthouses, La Jument, Masonry, Structural response, Waves loading, Breaking waves, R-PE UHPFRC, FEM, NLFM, Dynamic response

Résumé

Le présent travail a pour objet l'étude du comportement dynamique du phare de la Jument d'Ouessant, en France. C'est un ouvrage historique vieux de 111 ans qui fait partie du patrimoine de signalisation maritime, et qui soumis à des houles déferlantes. L'analyse s'effectue par le logiciel DIANA en utilisant la modélisation 3D aux éléments finis.

Le modèle est défini sur la base des dimensions structurelles et des matériaux, à partir de l'informations provenant des archives. Il est calibré sur la base de données collectées à partir d'accéléromètres et de documentations photographiques provenant d'une campagne de mesure réalisée à la Jument en hiver 2018 pour la plus haute vague enregistrée (19 mètres).

Les paramètres de réponse structurale (accélérations et déplacements) sont reproduits par des calculs éléments finis et sont comparés aux mesures in-situ de janvier 2018.

La relation entre les caractéristiques non linéaires des vagues déferlantes et la réponse structurale du phare est étudiée en évaluant l'effet de trois paramètres principaux : la magnitude du choc impulsive (effet de Gifle), la hauteur de l'impact, et le niveau de la marée.

Les prédictions du modèle sont comparables aux mesures réelles, ce qui confirme l'hypothèse principale de cette étude. Le modèle suggère que la magnitude de pression la plus probable de l'effet de gifle est de 230 kPa.

Finalement, un concept d'entretien composé d'une méthode d'intervention avec du BFUP et d'un plan de monitoring est proposé afin d'assurer la préservation de ce patrimoine historique et de son potentiel technique.

Mots-clés : Phare en mer, La Jument, analyse dynamique, éléments finis, sollicitation houles déferlante, analyse non-linéaire, BFUP

Table of Contents

List of Figures

List of Tables

List of symbols

- CD: Chart Datum corresponds to the lowest astronomical tide
- Hs: Wave significant height: The significant height is the mean of the largest one third of waves height in a wave record data
- D: Diameter of the cylinder or the lighthouse
- U: Speed of wave particles
- ρ: Water Density of the water
- d_b: Water depth
- L: Wave length
- H_b: Wave height
- R : Radius of the cylinder
- V: Speed of the wave
- Δ_z : Vertical extent of the impact
- Tp: Wave period
- η_b: Crest elevation
- f_{ute}: Tensile Elastic limit
- f_{utu}: Ultimate Tensile strength;
- ε_e: Elastic strain;
- ε_u: Ultimate strain

1 Introduction

1.1 Context and motivation

Ancient lighthouses have a phenomenal cultural significance. They were built as physical aid for navigation to guide mariners and to warn them from dangerous shallow rocky reefs. Therefore, protecting and preserving them is essential in case of Global Positioning System GPS absence.

''La Jument'' lighthouse lies about 3000 m off the coast of the isle of Ushant in the Iroise sea which is a part of the larger Atlantic Ocean between Ushant Island and Sein island, Figure 1. The Iroise sea is known as one of the most dangerous in the world, with violent and extreme waves and is also a popular area for tourism, sailing, commercial fishing and other activities. It is located in Brittany's coast at the north-western end of France, adjoining the busy trade and shipping route between the Atlantic, and the English Channel and North Sea.

On 20 February 1904, it was officially decided to build a lighthouse on a rock called Ar Gazec which means ''La Jument'' in Breton language, after numerous deadly shipwrecks at the entrance of the 'Fromveur' channel. La Jument became famous after many dramatic pictures taken by Guichard in a series of photographs to capture the giant waves hitting the lighthouse during a storm in December 1989 [1].

Numerous lighthouses at sea have withstood violent extreme environmental conditions for more than 100 years. Therefore, they are becoming a great opportunity for researchers to better understand their long-term stability against slamming impact of extreme waves and to preserve their outstanding cultural patrimonial values as well as to elucidate some challenging waves impact characteristics.

In this context, a collaboration was initiated in 2011 between MCS/EPFL and CEREMA Brest to study lighthouses at sea, and propose innovative techniques to reinforce them [3-4-5]. Most recently the impact of a giant wave on la Jument was monitored and documented photographically in January 2018 [3-4].

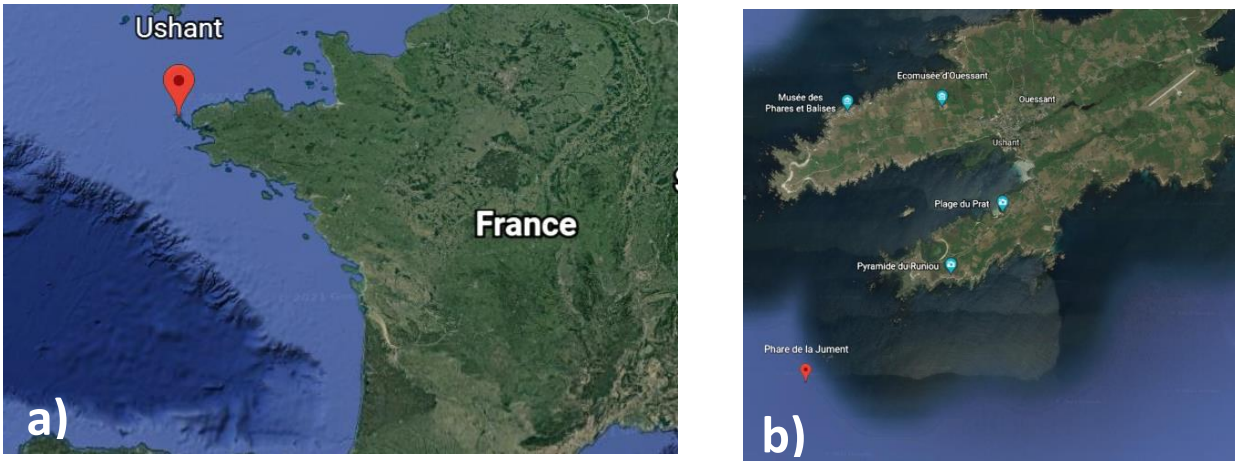

Figure 1:a) Ushant Island Location in the Iroise sea; b) La Jument lighthouse location [Google Earth]

1.2 Objectives and research approach

Understanding the structural response of offshore lighthouses under waves loading is a challenging but important task. Most of the existing research about lighthouses structural response are performed on field or laboratory measurements whereas limited work is based on FEM simulation [4-5-6-7]. Putting the experimental and modelling approaches together is fascinating and requires adopting logical hypothesis supported by literature.

The aim of this project is to study the structural response of ''La Jument'' lighthouse under extreme waves loading in particular the highest wave event of 19 meters height that happened during a monitoring campaign in January 2018. The characteristics of waves impacting la Jument during a winter storm in 2018 were described by Filipot [2]; Denarié [3] further analyzed the accelerometers measurements and characterized the in-situ dynamic response of La Jument.

Thus, the first objective of this study is to reproduce the structural response parameters (acceleration and displacement) under the action effects of a breaking wave by 3D finite element modelling (3D FEM) analysis using the commercial software DIANA and to compare them with the actual in-situ measurements. The second objective is to propose a reinforcement using Ultra High-Performance Fiber Reinforced Concrete (UHPFRC) with synthetic fibers to protect la Jument lighthouse. The third objective is to propose measurement campaigns to improve the understanding of breaking waves impact pressure.

1.3 Thesis outline

The thesis report consists mainly of 9 chapters. Following the introduction of the project's context and objectives, the second chapter describes the historical context of la Jument lighthouse and includes the main reinforcements since its commissioning in 1911.

The third chapter covers the acting loads, in particular waves loading. The theoretical background of breaking waves characteristics, their slamming actions, and their vertical and horizontal distributions are also discussed.

The fourth chapter describes the in-situ experimental measurements performed at La Jument and discusses the extreme wave event considered for this study and its classification

After discussing the main hypothesis of FEM analysis and the modeling procedure in the fifth chapter, chapter six provides the natural frequencies analysis of the lighthouse as well as the calibration of the model parameters. The seventh chapter characterizes the dynamic behavior of la Jument under the actions of a 19-meter wave with various characteristics and includes the superposition of experimental results and FEM calculations.

The eighth chapter proposes a concept of maintenance which combines an intervention method using the UHPFRC and a proposal for a measurement campaign. Discussion and conclusions of the research can be found in the last chapter.

2 Historical background

2.1 Construction and materials

The historical design of lighthouses was very empirical due to lack of knowledge of the complex waves' characteristics. It was based on trials and overestimated safety considerations such as massive characters to ensure strong and durable structures resisting remarkable oscillations.

La Jument Lighthouse was constructed between 1904 and 1911 and triggered by the 400 000 francs Charles Eugène Potron legacy. The lighthouse has sustained in 2021 more than 110 years of extreme environmental loadings. The equivalent access time for construction during the 7 years of construction was approximately 85 days. Access time is very limited by weather conditions (storm Surge) as well as tides. The south-west view in April 1906 is illustrated in figure 2 a.

After reviewing the archives, it was concluded that the outer skin of the tower is made up with natural granite stones with 40 cm of thickness except the lower part of the tower with 60 to 80 cm thickness. The sources of those stones are two quarries located along the coast (Kersanton and Laber). The materials were chosen to be durable and to resist severe waves. However, the interior part of the tower was built by a masonry of coarse stone blocks with dimensions around 15 to 20 cm manually jointed by means of cement mortar. This masonry can be compared to a dam concrete referred as non-reinforced concrete in this study, figure 2 b.

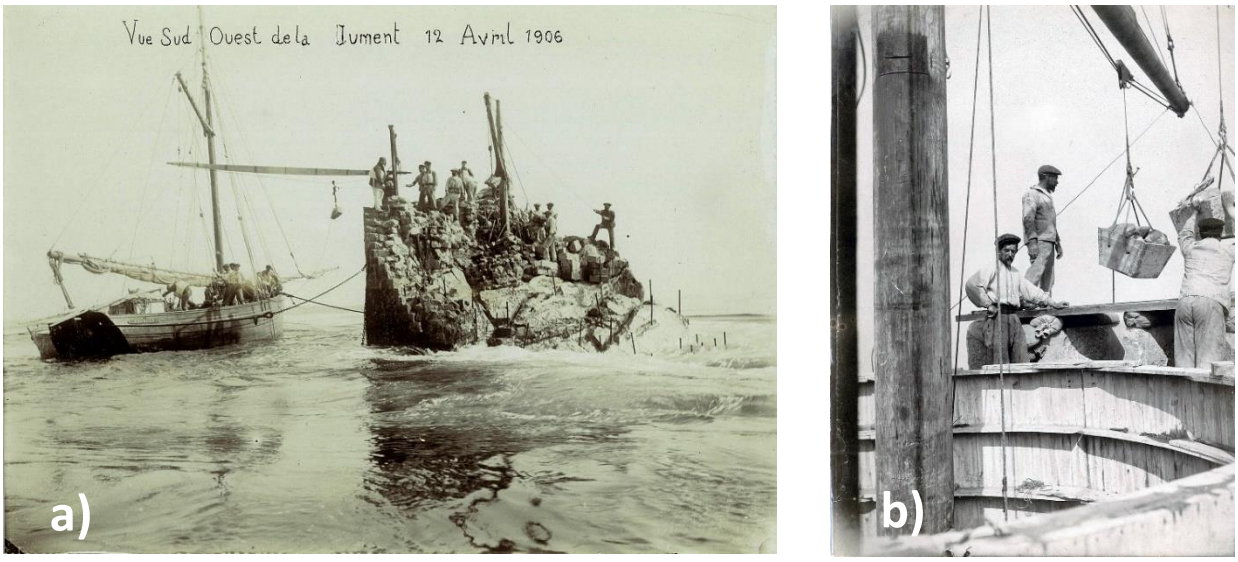

Figure 2:a) Base construction, South-west view April 1906; b) Masonry and mortar [Loïc Malgor]

2.2 Reinforcements

Various essential reinforcements were realized for stabilization purposes throughout the history of the structure as described below. The information mentioned in this section was extracted from the Quimper archives.

The first reinforcement was widening the basement by about 1 meter in the north western direction shortly after the structure was commissioned in 1911. However, it was loosely connected with the rock foundation. This was initiated after the lantern glass was cracked due to remarkable vibration caused by giant waves and severe storms in December 1911.

The second reinforcement was a reinforced concrete ring to improve the resistance against storms waves from level +10.5 m till +18 m Chart Datum CD. Giant waves were not observed to be higher than 18 meters at that time. The motivation for this RC ring was a main horizontal crack appeared in the lower part of the tower at level +11.4 m CD after the storm of November 1915, as reported by the keeper. Furthermore, there was some masonry edge spalling. Therefore, the storm generated a fatigue state in the masonry due to alternating forces between extension and compression whereas the upper part of the lighthouse was intact, and no cracks were initiated. Another external crack appeared at the level 15.25 m which was might be extended to the inside of the tower. Therefore, the main role of the reinforced concrete ring was to prevent this crack from spreading all over the tower (Cracks confinement) and to take the stresses produced by breaking waves. However, their intention was not to increase the tower stiffness.

The third reinforcement was the enlargement of the base of the tower for the 2nd time between 1919 and 1928 following many storms that induced violent vibrations in the tower. The reinforcement consisted of widening the old base by 2.5 m from the south direction with reinforced concrete which was later covered by masonry. The base was also raised also by 3.5 meters until the level +14 CD and anchored to the bedrock. The cavities between the old base and the bedrock were filled. Thus, the main objective was stabilization of the tower to prevent significant oscillations.

The last main reinforcement was performed between1936-1941 following the engineer Coyne's propositions. The idea was to anchor the lighthouse tower in the basement by post tensioned anchors inclined 1/ 10 towards outside. In the original project, 6 anchors were planned. However, 3 anchors were executed. The first was in 1936 and the others were in 1941. Their planned function was to add vertical compressive forces to add stability to the tower, up to around 4800 tons. In fact, it is applying stabilization forces originally designed as 3 by 1000 Tons but the effective loads executed was around 1600 tons. The real efficiency of the cables is questionable as their anchorage could not be verified. Furthermore, they might be corroded after 80+years due to the salty aggressive environment.

To sum up, the original height of the lighthouse's tower was 29.7 m and with a substructure of 10.5 m. This base was widened and raised by 3.5 meter which decreased the tower's free height to 26.2 m. The top of the old base was at +10.5 m CD whereas the top level of the new widened base is +14 m CD. CD: Chart Datum, equivalent to the lowest astronomical tide.

Furthermore, the lighthouse is distinguished by its atypical shape and is composed mainly of the substructure and an octagonal tower which is composed of 7 levels (Entrance, Kitchen, 3 rooms, honorable guests' room, and technical room). A lantern made up of steel is constructed at the top of them. A corbel at the top was necessary to increase the size of the technical room. The optics system in the lantern was Fresnel lens with a range of 22 miles before its replacement in 2014 by a LED light source with a range of 10 miles. These details are illustrated in figure 3 and 4.

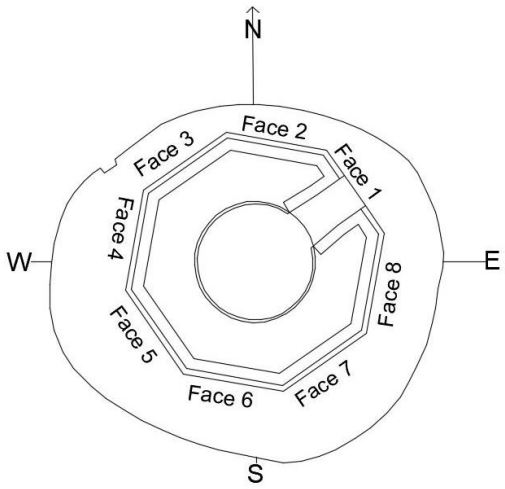

Figure 3:La Jument Lighthouse Top view

Figure 4: Vertical section: Reinforcement details

At the lowest tide level, 2 meters approximately of the rocky foundation can be seen whereas at the highest tide level, the upper level of the substructure is almost 6 meter above sea water level. In figure 5, the top level of the original base before rising +10.5 m CD is indicated by the red arrow +10.5 m CD. The top level of the base after reinforcement is at + 14 m CD whereas the top level of the reinforced concrete ring is at +18 CD m.

Figure 5: La Jument [Ronan Follic]

Figure 6 shows the rocky foundation of La Jument at the lowest tide level (+0.00 CD). More details about the actual state of the lighthouse such as cracks and damages are fully described in section 8.2.

Figure 6: Rocky foundation of La Jument at the lowest tide level [Nicolas Fady]

3 Acting Loads

3.1 Overview

Numerous Loads are acting on the lighthouse whether they are permanent or transient. Action effects of waves loading are predominant. Wind loads are not taken into consideration in this study as they represent only a risk for nonstructural elements such as the lantern and the windows but have negligible effect for structural elements. Seismic loading is also not considered as the seismic risk for this region is moderate.

Lighthouses were designed based on instinctive waves loading in the 19th century due to the lack of knowledge in wave breaking phenomena. However, they have survived extreme environmental loading for more than one century. Thus, their safety consideration was overestimated to ensure serviceability of the lighthouse.

The aim of this section is to introduce waves loading and to focus mainly on the significant pressure caused by the extreme waves.

3.2 Waves loading description

Waves-structure interaction is affected by different factors such as tide level, wave velocity, weather conditions, waves period, crest height, and other.

The force exerted on circular piles exposed to waves in deep water was estimated by Morison [8]. This formula is generally valid for non-breaking waves hitting slender cylinders with the ratio of wavelengths to member diameter larger than 5. The total force which varies in function of the water surface elevation is expressed as a summation of inertia force F_I and drag forces F_D. It is referred as the quasi-static component of waves actions expressed in equation 1 for a vertical slender pile on a uniformly sloping reef [8].

$$F = F_I + F_D = C_I.\rho.\frac{\pi.D^2}{4}.\dot{u} + C_D.\rho.\frac{D^2}{2}.u.|u| \quad \textit{Equation 1}$$

where C_I is the inertia coefficient, C_D is the dynamic coefficient, D is the cylinder diameter, U is the particles speed, and ρ is the water density.

The total wave forces exceed, however, the value predicted by Morison. This is confirmed by experimental results of waves forced exerted on vertical cylinders [9-10-11]. This increase in the force is due to the slamming impact of breaking waves. Therefore, additional dynamic component is added to represent the slamming effect. Several studies concerning waves loading on vertical cylinders [9-10-11] with 3D test provided different expressions for the dynamic component despite its complexity.

3.3 Breaking waves

The type of breaking significantly affects the severity of the wave action effect and its pressure impact on the structure [12]. There are many types of breaking waves such as spilling waves (most gentle), collapsing, surging, and plunging waves.

The plunging waves illustrated in figure 7 occurs when the wave breaks immediately in front of the cylinder. They are characterized by a steeper crest and more intense jet enclosing an air pocket when breaking. The aeration effect on the impulsive pressure time history plays a major role. The highly aerated front face will cause a lower impact force whereas non-aerated front face induces higher impact due to the high fluid velocities [13].

The height of breaking can increase up to a physical limit called steepness and approximated by Miche [14] in equation 2. The waves become unstable beyond this height and they release their energy by breaking.

$$\frac{H_b}{L} = 0.14 \times \tanh\left(2 \times \pi \times \frac{d_b}{L}\right) \quad \text{Equation 2}$$

where d_b is the water depth, L is the wavelength and H_b is the height of the wave.

The seabed formation around the lighthouse is a major factor for waves breaking. Wienke [15] assumed that the waves break when the particles velocity in the crest reach the waves velocity. Usually the breaking phenomenon occurs at a relatively short distance around (20% to 40% of the wave height) from the structure [16].

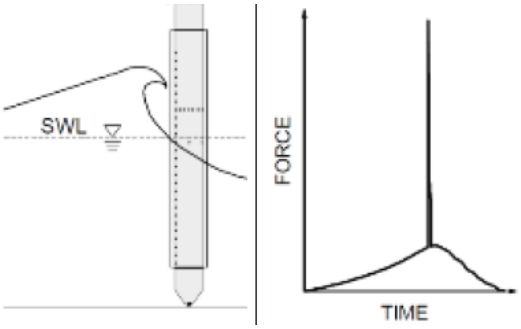

Figure 7: Plunging Breaker, Dynamic and Quasi-static Component [15]

3.4 Rogue waves

The most severe type of plunging breaking waves is rogue waves. There is a lack of proper understanding of their physical characteristics due to scarce observational field data. They are one of the most challenging aspects to investigate but they are essential for the design of off-shores structures. The first rogue wave detected by measuring instruments was the Draupner wave on 1/1/1995 in the North Sea [17]. This 25-meter wave with a crest height of 18.5 m was the subject of numerous researches to understand the complex phenomenon of rogue waves.

Rogue waves are characterized by significant high pressure, short duration (milliseconds), with nonlinear characteristics. They are defined by Haver [18] with some empirical criteria. The most popular one is when an observation revealed a wave height that is greater than 2 times the significant height Hs. It can be defined also if the crest elevation is greater than 1.25 times the Hs.

3.5 Slamming pressure calculation

The slamming pressure can cause severe damages to lighthouse. Calculating this pressure is an ambiguous task due to the non-linearity of the rogue waves' phenomenon. It is governed by the air, water, structure interactions

The Von Karman theory [19] was the first attempt to calculate this impact force on cylinders but with infinite length with the following expression in equation 3.

$$F(t) = \rho.\pi.R.V^2\Delta_z\left(1 - t.\frac{V}{R}\right) \textit{ Equation 3}$$

Where the R is the radius of the cylinder, ρ is the water density, V is the wave's speed, Δ_z is the vertical extent of the impact.

The wave velocity for plunging wave can be approximated as the square root of the gravitational acceleration multiplied by the wave height as in equation 4

$$V= \sqrt{(g} \times H_b) \textit{ Equation 4}$$

The theory of Wienke & Oumeraci [11] is mainly the basis of ISO 21650 'Actions from wave and currents on coastal structures. They proposed a dynamic component formula to calculate the maximum impact pressure when the waves break in front of the cylinder. The proposed impulse force is about 70% of the one calculated by Von.

The time of slamming is given in equation 5 which in fact lower than Goda's estimation

$$T = \frac{13}{32} \times \frac{R}{V} \textit{ Equation 5}$$

Despite the fact that experimental studies are limited to laboratory conditions such as the geometry, the water depth and the typology of the reef, they can help in estimating the slamming pressure magnitude. According to [20], breaking waves can create slamming pressure in the order of 200 kPa for milliseconds that leads to brittle fracture of mild steel. Recently, experimental test with computational fluid dynamics method and numerical simulation of an offshore platform under rogue waves were performed by [21] in 2021. [21] confirmed that the slamming pressure for a 20-meter wave with a period of 11 seconds is between 220 and 250 kPa equivalent to 22.4 t/m^2 and 25.4 t/m^2 respectively with an average allowable error of 2.5 %.

3.6 Horizontal and vertical distribution of waves loading

3.6.1 Horizontal distribution

Several analytical approaches proposed the estimation the pressure distribution around the perimeter of a circular cross-section.

According to laboratory tests on cylinders subjected to different types of waves, it was possible to observe the rapid decrease in pressure when moving away from the point perpendicular to the wave's direction. The pressure becomes quasi null if the angle is 45° with the perpendicular direction to the incoming wave [9]. The same results were provided by [11] in a parametric study considering 7 different locations around a cylinder. Therefore, the horizontal pressure distribution can be calculated in function of the of the angle with the perpendicular direction to the incoming wave (azimuthal distribution). The pressure measured around vertical cylinder is 70% of the load if the angle is within ±15 degrees and 30% if within ±30 degrees. It is illustrated in figure 8.

As for the octagonal tower, it was challenging to estimate the load distribution. The pressure for the face perpendicular to wave direction must be fully applied, whereas for the 2 adjacent faces oriented 45 degrees, a portion of the maximum pressure must be taken. This portion is approximated by 65% by [4] and it is much larger than cylindrical towers.

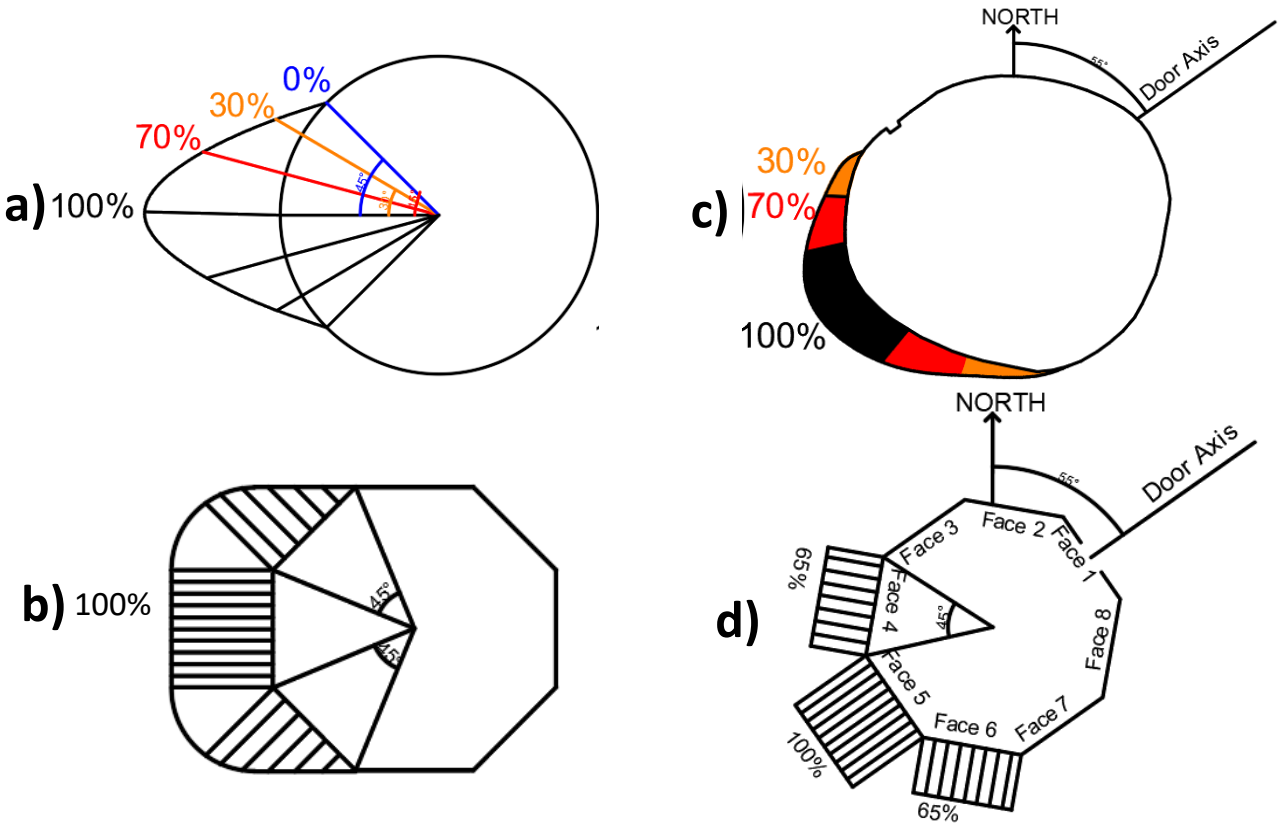

Figure 8: Horizontal distribution of the pressure: a) and b) Theoretical distribution [19]; c) La Jument basement distribution and d) La Jument octagonal tower distribution

3.6.2 Vertical distribution

The load must be distributed between the crest and the trough of the wave. [10] estimated the impact area by an empirical coefficient which is the curling factor λ = 0.4. [11] proved that the curling factor depend on the breaking type which means the shape of the wave just before impact. It is approximated by 0.46 according to experimental testing on cylinders under plunging breakers and 0.22 for spilling waves. η_b is the crest elevation which is 80% of the wave height by [10] and 95% by [22]. Therefore, the height of impact area is given by equation 6 as shown in figure 9.

Height of Impact area= $\lambda.\eta_b = \lambda \times 0.8\times H_b$. Equation 6

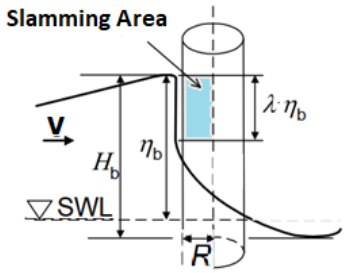

Figure 9: Breaking on a cylinder: Impact Area [15]

The impact area is divided into 2 main domains. One corresponds to the slamming impact on top of the other that corresponds to the compressive impact described by [23]. The compressive impact caused by the sudden compression of the air enclosed between the impact area and the concave front of the breaking wave happens directly after the slamming.

The maximum pressure is expressed by the following equation:

$$p_{max} = p_0 + 2.7 \times \rho \times V^2 \text{ Equation 7}$$

where $p_0$is atmospheric pressure, ρ is the water density, V is the speed of the wave.

The same phenomenon was described earlier in 1969 by [24], figure 10.

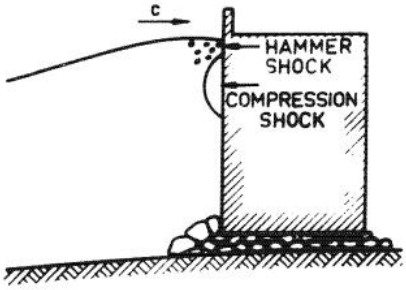

Figure 10: Dynamic Impact [24]

4 Case Study: Extreme wave event 2018

4.1 In-situ experiment at La Jument

A study is conducted at la Jument to better understand wave breaking and their effect on the structural behavior of the lighthouse. The deployed instruments were X band radar, Stereo-Video Imagery system (SIS) and four accelerometers during a monitoring campaign in winter 2017-2018. The 4 accelerometers RECOVIB-IAC-A03 are installed in different orientation and along the height of the lighthouse at 4 different positions +20.6 m, +31.1 m, +38.7 m, +45.6 m CD illustrated in figure 11. Their sampling rate is 250 Hz with a arrange of ± 2g [3]. [2] described several storm waves, acceleration observation as well as collected bathymetric data during this monitoring campaign. However, the focus was on the characteristics of a specific Giant waves of 19 meter. It was the only wave that induced significant accelerations in the lighthouse. This wave occurred on 3 January at 9:42:07 UTC in which the lighthouse exhibited strong vibrations. The same name '' Wave 1'' given for this special wave by [2] and [3] is used in this report.

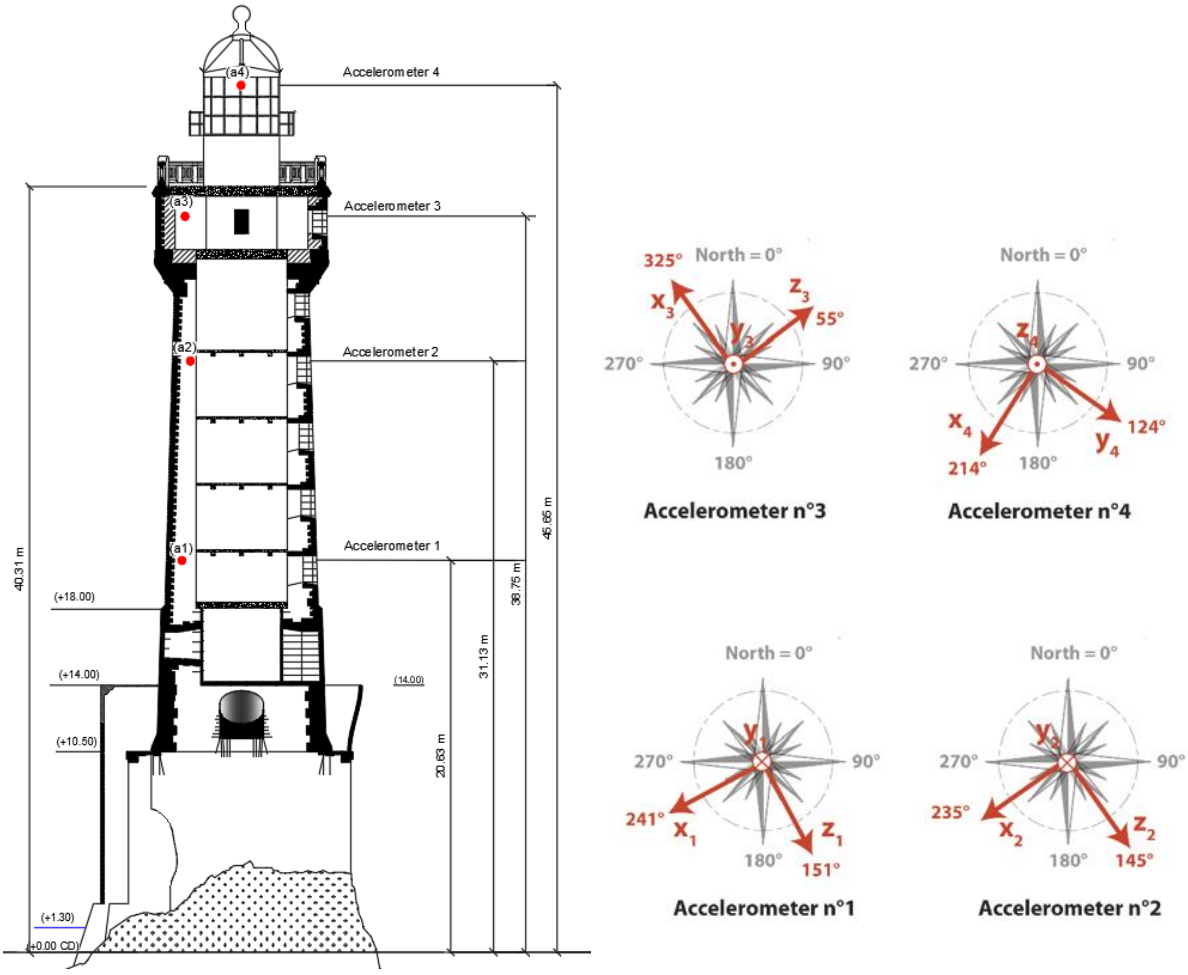

Figure 11:Accelerometers position and orientation [3]

4.2 Wave considered for FEM analysis

The aim is to reproduce the structural response parameters of La Jument by FEM simulation and to compare them with the actual measurements. The wave considered for this study is **wave 1**.

There are 2 scenarios of the wave 1. The first is mentioned by Filipot [2] according to the monitoring system. The 19-m wave has a crest of 12.9 m and a trough of 6.1 m. The crest height is approximately at the same level of the substructure (+14 m CD) and the likely orientation of the wave is **NW**, hitting face 4 approximately. The second scenario of wave 1 mentioned by Denarié [3] is actually from the photographical documentations of the breaking wave and the analysis of the accelerometers data to find principal directions of accelerations. The pictures were taken at the moment of the breaking by 2 different photographers at 2 different positions. They proved that the wave was hitting the tower at the upper level of the reinforced concrete ring (~+18 m CD) with a most likely direction of **WNW** hitting, in particular the corner of Face 4 and 5 illustrated in figure 14. The wave is assumed hitting face 5 in this study.

What makes Denarié scenario more accurate is that the photographical documentations are taken at the moment of slamming on the lighthouse whereas monitoring systems do not give access to the impact zone. The characteristics of the 19-meter wave were determined 50 meters away from the lighthouse which was the range of the Stereo-Video Imagery system.

Figures 12 and 13 illustrate wave 1 at the moment of breaking from two different locations. One of them is facing the sun light.

Figure 13: Wave 1 breaking [Dominique Boat]

Figure 12: Wave 1 breaking [3]

In fact, the 2 scenarios are equivalent. Waves characteristics such as its speed and shape (crest height) determined at a certain distance from the lighthouse does not imply it will remain the same when arriving the vicinity of the lighthouse.
The sudden rise of the reef increases the non-linearity of the wave when approaching, and therefore, the crest elevation can change notably over distances as well as wave's speed.

The sea floor depth is derived by a sonar system when approaching the lighthouse along the main axis of the door with a 55° azimuth as shown in figure 14.

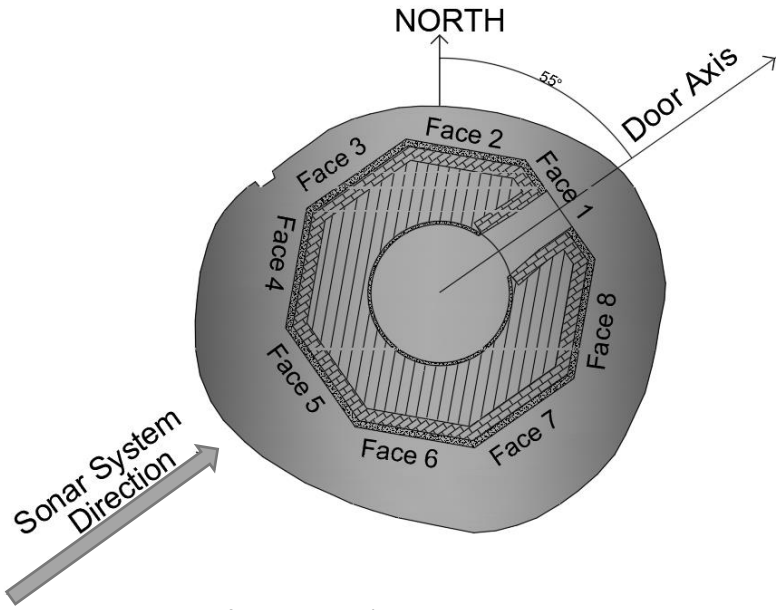

Figure 14: Top view of La Jument (Octagonal tower and substructure)

The data was obtained by a compilation of sonar measurements from a fishing boat from the island [25]. The + 0.00 Chart Datum is approximately 1 to 2 meters below the top of the rock.

Figures 15 and 16 show the sea floor for the first 351 meter away from the lighthouse with 60 meter in depth and 30 meter in depth respectively. The orange arrow represents approximately the furthest south western end of the lighthouse.

As can be noticed, there is significant increase in the rocky reef when approaching the lighthouse. It is approximately 52 meters over a distance of 352 meters and in particular 22 meter over a distance of 50 meter away from the lighthouse. Therefore, this sudden drop in the rocky foundation of La Jument on its southern-western boundary justifies the non-literality of the approaching waves and confirm the photographical documentations scenario.

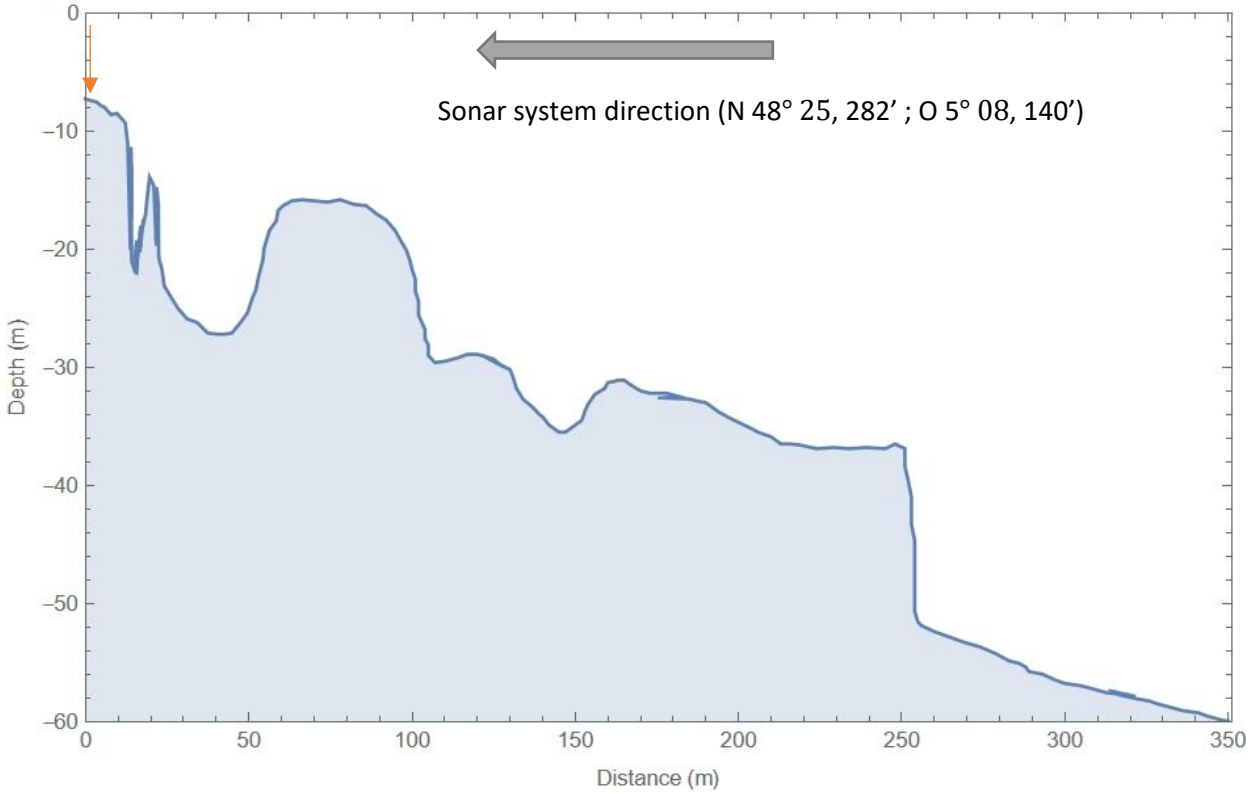

Figure 15: Sea floor depth along the lighthouse door's axis (60-meter depth)

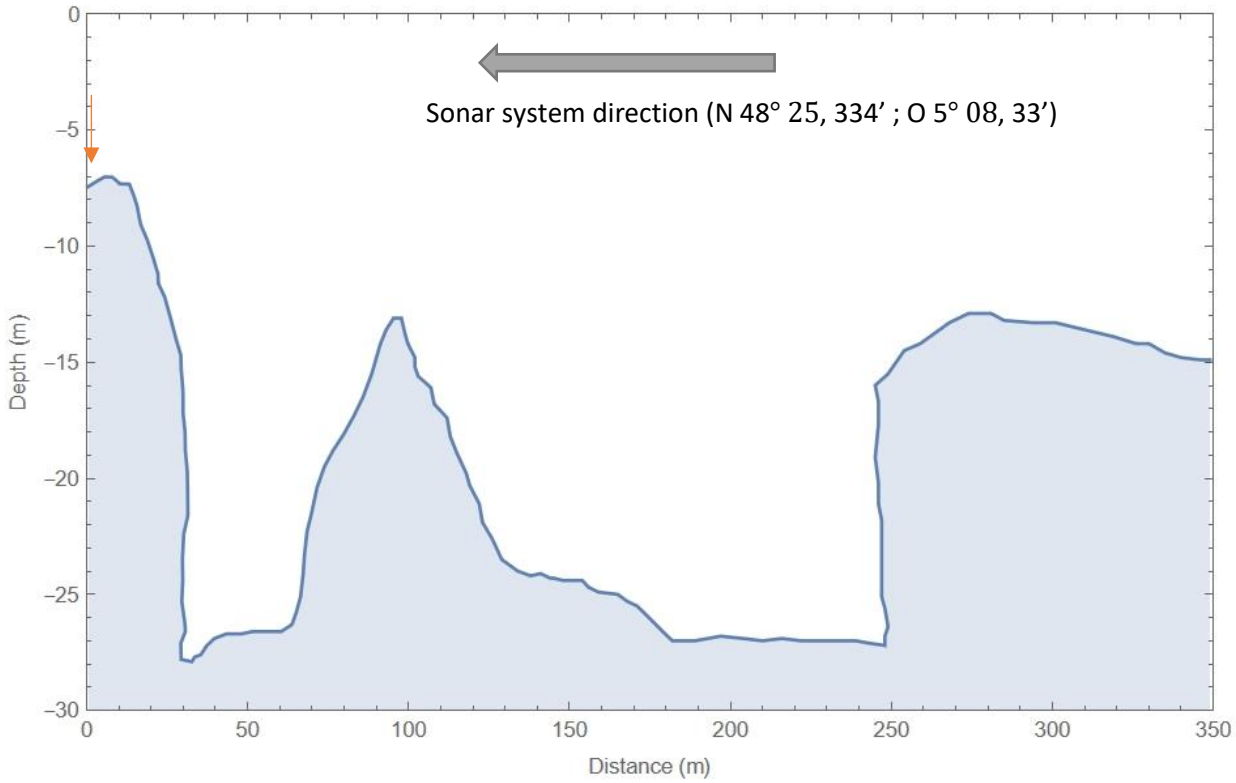

Figure 16:Sea floor depth along the lighthouse door's axis (30-meter depth)

4.3 Wave 1 Classification

The wave 1 is classified as a rogue wave. It satisfies one of the empirical criteria mentioned in 3.3 (η_b >1.25×H_s) and its wave height is almost double the significant height.

In the following Table, the main characteristics of wave 1 are compared to those of the Draupner wave which is the first rogue wave detected by measurements.

Table 1: Waves Parameters Comparison between the Draupner wave [17] and Wave 1 [2]; Hs is the significant height, Tp is the wave period, H_b is the wave height, and η_b is the crest elevation.

Wave parameters	''Draupner wave'' 01/01/1995	''Wave 1'' 03/01/2018
H_s (m)	11.9	10.0
T_p (sec)	14.4	13.3
H_b (m)	25.6	19.0
η_b (m)	18.5	12.9
η_b/H_s (-)	**1.6**	**1.3**
H_b/H_s (-)	**2.2**	**1.9**

Water level estimation is essential in coastal engineering and it depends on many factors such as astronomical tides and storms surge. The tidal level is related to the tide's coefficient. The higher the tidal coefficient, the larger the tidal range. The storm surge is related to atmospheric pressure and defined as an abnormal rise in sea water level during storms. The significant height is the mean of the largest one third of waves height in a wave record data.

The dependency of wave height on tide level is weak whereas the dependency of wave height on storm surge is high because storms often generate giant waves. However, tide level affects the position of applying the wave force. For a low tide level, the waves would break mostly on the base of the lighthouse, for example, whereas with a high tide level, the waves would break on the tower with much higher actions effect.

The maximum tide level that corresponds to 120 tide coefficients is +8.2 m CD. The tide level when the breaking of wave 1 occurred (9:42 UTC) was around +1.3 m CD whereas the mean tide level in 3 January 2018 was 4.13 CD which corresponds to a return period of 0.8 years approximately. Moreover, the significant height for this event was 10.0 m which corresponds to a return period of 2 years. [Appendix 2]. The storm surge at that day during the event was too small around -0.2 m and therefore, the sea level is not affected notably according to many specialized websites. [26].

Therefore, the event of 3 January was not an extreme event but a severe one and the breaking mode considered for this study is plunging breakers.

5 Finite Element Modeling

5.1 Structure Modeling and Challenges

The modelling is performed using the commercial finite element software DIANA. The historical archives were summarized by [4] to get the structural dimensions and materials of La Jument lighthouse.

The lighthouse's model was previously created in Holland with the help of TNO DIANA in Delft back in 2012. It was modeled using the combination of two software. The first FX Midas+ works as pre and post processor and the second DIANA 9.4 is for calculations. However, FX+ Midas and eth 2012 model are no longer compatible with the current version of DIANA 10.5.

The main focus in this section is to recreate the same conditions of the previous model while taking into consideration the major differences between the old and new version of the software. After that, a parametric study is performed. The major difference is mainly the method of defining the loads and the boundary conditions. Previously, the loads pressure can be applied on a set of selected elements whereas in the new version, the load must be applied to predefined geometrical sections.

Therefore, the challenge in this project consists of 3 main tasks: 1) Importing the model from DIANA'S previous version, 2) Defining the materials constitutive model and boundary conditions, and 3) Modeling the wave.

Some main simplifications of the model were mentioned in [4] 1) the 10 cm slabs rigidity inside the tower were neglected, 2) the openings were modeled without worrying about the exact shape, 3) The steel lantern is not modeled, 4) The rock foundation of the lighthouse is modeled with an average thickness of +2 m CD and not with its exact shape ,and 5) Reinforcement in the base is not modeled due to the uncertainties about their execution plan. Those main assumptions are re-checked according to the archives and discussed again with the supervisor. They are all logical to proceed with and they save numerical calculation time.

5.2 Materials characteristics

DIANA FEA requires several parameters which include linear material properties along with parameters that affect cracking and damping phenomena.

The development of cracks causes the non-linear behavior of materials which are defined with the multi-directional fixed crack model (MFCM) in DIANA. There are several models integrated with DIANA to characterize the tensile behavior of the masonry such as Linear Tension Softening, Multilinear Tension Softening, Exponential Tension Softening, among others.

The choice of the Hordijk model [27], which is expressed in equation 8, is convenient for the masonry's nonlinear characteristics because it characterizes the softening branch of the stress stain curve and is simple and stable for calculations. It proposes a crack stress equal to zero at an ultimate crack strain and has a low tensile range 0.3 to 1MPa but with a softening behavior once the tensile limit is reached. Furthermore, this model is simply defined by the tensile strength and the specific fracture energy in DIANA. Using this model is recommended for the convergence of the calculation. It is illustrated in figure 17.

$$\frac{\sigma}{f_t} = \left(1 + \left(C_1 \frac{\Delta u_n}{\Delta u_{n,ult}}\right)^3\right) e^{-C_2 \frac{\Delta u_n}{\Delta u_{n,ult}}} - \left(\frac{\Delta u_n}{\Delta u_{n,ult}}(1 + {C_1}^3)\right) e^{-C_2} \quad \textit{Equation 8 with } C_1 = 3 \textit{ and } C_2 = 6.93$$

$\Delta u_{n,ult}$ is the crack width at which no more stress is transferred $\Delta u_{n,ult} = 5.136 \frac{G_F}{f_t}$

G_F represents the specific fracture energy which is the area under the curve

f_t: is Tensile strength

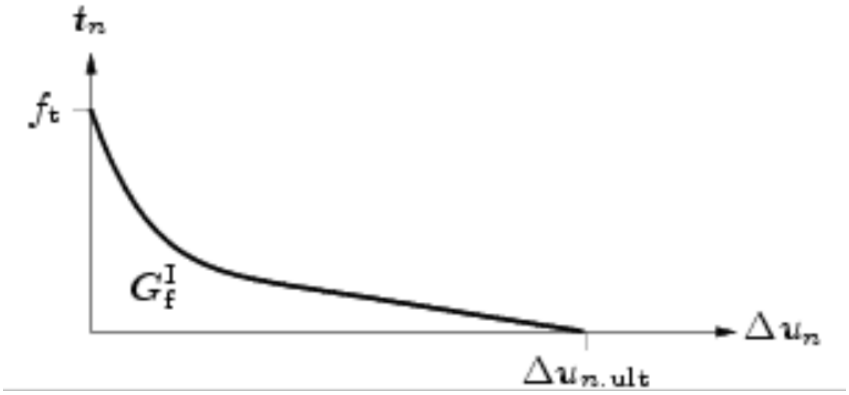

Figure 17: Softening model Hordijk 1992 Model [46]

The materials definition requires a shear retention factor which refers to the amount of shear transmission across a crack. It must be between 0 and 1. If it is 1, the failure mechanism would change from shear to flexural. This value is overestimated and does not represent the actual state of the concrete or masonry. The shear stress transmitted across the crack decrease with the increase of cracks strains [28]. The default value by DIANA is 0.01. It is actually relating the stiffness after cracking and initial shear stiffness. Therefore, for this project, a conservative retention factor of 0.01 is assumed and it is seeming to be convenient.

The Rayleigh damping parameters were calculated based on the accelerometers data analysis at La Jument in January 2018 [3]. The damping was found to be 5% which is typical damping for concrete and masonry structures. More details are discussed in section 6.4

It is worth mentioning that the softening of the upper part of tower is not considered because It is more likely that this part will not exceed its elastic range. This saved calculation times.

Furthermore, to localize the cracks in plane, a weak masonry layer of 50 cm at the lower part of the inner tower was originally created in the previous version with a smaller softening behavior due to a numerical artifact causing a non-existing diagonal crack [4].

In DIANA 10.5, this problem did not occur and there was no need to model it. However, it was modeled due to uncertainties about the connection between the tower and the old base. Calculations proved that there is no effect on the displacement and acceleration.

The materials characteristics used in the materials model definition are summarized in table 2 and a vertical cross section as modeled in DIANA is illustrated in Figure 18.

Table 2: Materials characteristics summary [E: Modulus of elasticity, ρ: Density, v:Poisson's ratio, ft: Tensile strength, and Gf: specific fracture energy [4]

Materials	**E [GPa]**	**ρ [Kg/m^3]**	**ν [-]**	**f_t [MPa]**	**G_f [J/m^2]**
External Masonry layer	10	2600	0.2	0.3	20
Non-reinforced concrete (Masonry + Mortar)	10	2500	0.2	2	100
Masonry of the substructure (Before and after reinforcement)	10	2500	0.2	1	100
Weak masonry	10	2500	0.2	0.8	40
Elastic masonry	10	2600	0.2	-	-
Steel Reinforcement	210	7850	0.3	-	-
Rocky Foundation (Elastic Gneiss)	60	2500	0.3	-	-

The modulus of elasticity is assumed as 10 GPa as a first step. Some other results are based on E= 15 GPa. This is fully discussed in section 6.2.

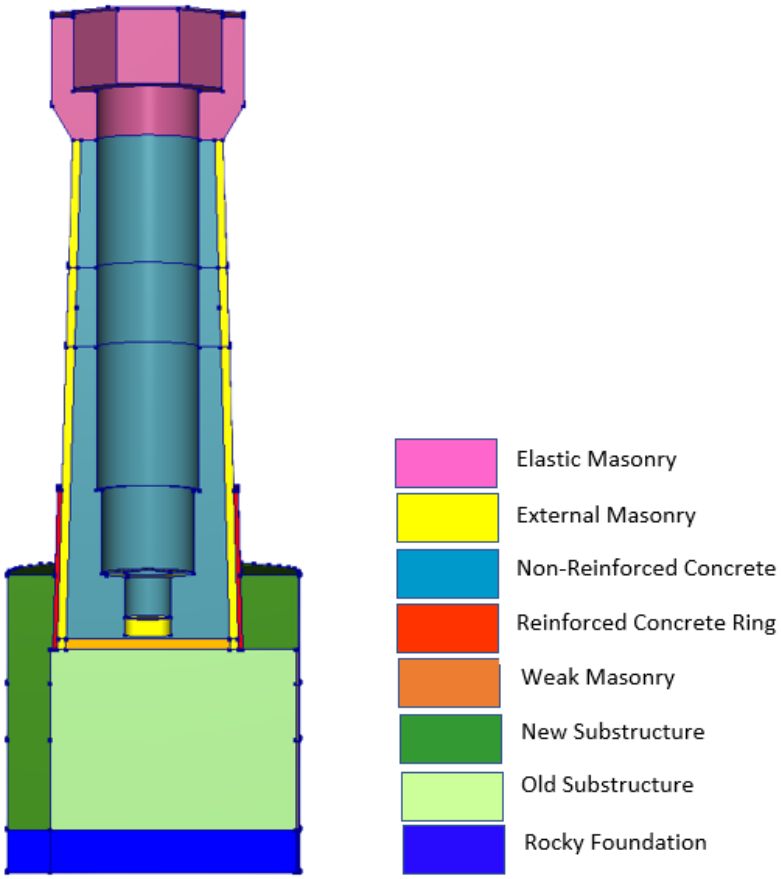

Figure 18:Vertical section with materials assignment in DIANA

5.3 Mesh assignment

The choice of a suitable mesh size is an essential part in the Finite Element model to get accurate results with the least time. The smaller the mesh, the more accurate the results are. A compromise must be done to balance between computation time and accuracy. Usually mesh size decreases around critical areas for better accuracy. The mesh previously modeled was tetrahedral solid elements whereas in the new model, hexahedral-quadrahedral mesh with a linear order is chosen given the complexity of the geometry and for more accuracy. Both mesh size of 50 cm and 30 cm of the element were tested for the new model and they give the same accuracy. Therefore, the selected size is 50 cm to minimize the calculations time to the half approximately. The number of elements is approximately 176000.

5.4 Waves Loads Modeling

The waves modeling mainly involve 2 parts: the specification of the load (horizontal and vertical distribution) and its association with a time curve (Pressure magnitude vs time)

There are 3 methods to apply the distributed load in DIANA 10.5 on a specific area along a specific height:

1) The area must be already modeled with the considered height
2) The area must be created every time with the change of the height of application
3) The load is defined in function of the height for a specific selected area (Space Function)

The first 2 methods are not practical for a parametric study whereas the 3rd method is practical because the height can be changed in a space function without editing the geometry. It is worth mentioning that in the model of 2013 [4], the pressure load can be applied by selecting the target elements which is easier but with a smaller precision ($\pm$25cm).

The structure under study is subjected to significant dynamic loads caused by rogue waves which are represented by a compressive impact followed by a slamming pressure.

As for this project, the wave loading in the vertical distribution is modeled as 3 main rectangular pressure blocks applied on the lighthouse as illustrated in figures 20 and 21. The upper 2 pressure blocks represent the dynamic pressure applied on the impact area mentioned in section 3.6.2 whereas the third lowest block represents the quasi-static component of the waves action. The quasi-static pressure has a negligible effect on the maximum displacement which is mainly depended on the wave impact. However, it is modeled in this study to get as closer as possible to the reality.

The dynamic pressure depends on the shape and time of breaking. In this study, a plunging wave breaking in front of the cylinder is considered. The pressure is applied on the impact area which is divided into 2 main parts. The first represents the slamming pressure (Slamming peak equivalent to Gifle peak in French) which is a concentrated force over a portion of the impact area. It is applied with an almost higher pressure than the second part and with 0.1 second difference. The second block corresponds to the compressive impact described in section 3.6.2.

The rise time given by [23] for the slamming pressure is in the order of 0.001 seconds and for the compressive impact is in the order of 0.1. [4] analyzed the acceleration and displacement by varying the rise duration between 0.001 s and 0.1 s for the dynamic impact on la Jument in a parametric study. As loading duration increases, the displacement and acceleration amplitude increases and rapid oscillation occurred when the loading time is less than 0.05. The mode 2 of natural frequency is predominant for impulse loading of 0.001. The structural response is greatly affected by the impulse nature. Thus, for this study, the rise time is taken 0.05 seconds for slamming impact.

Each pressure block is associated with a time function in DIANA. Pressure time relation is proposed to describe the 2 components of the wave impact [4]. The quasi-static pressure is taken as bilinear equation whereas the dynamic pressure is represented by a linear rapid load rise, followed by a pressure drop which follows an exponential decay law as in Figure 19.

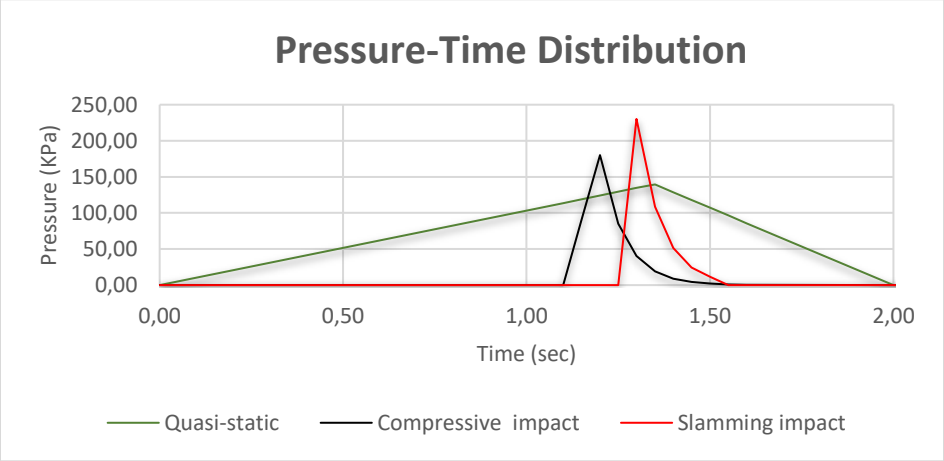

Figure 19: Pressure-Time distribution of waves loading

5.5 Analysis procedure and parameters under consideration

The structural response of the lighthouse depends on many factors related to the structure itself and to the waves' characteristics such as the type of waves breaking, the magnitude of the pressure, the impact duration, the impact area, and the tide level.

Dynamic analysis is required to investigate the structural response of the lighthouse. A non-Linear structural analysis is defined with time steps which must be input based on the time function associated to the waves loads to get accurate results.

Numerous factors affect the structural response of lighthouses under waves action. The essential governing parameters assessed in this study are: 1) Impact pressure magnitude, 2) Portion of Impact area allocated to slamming pressure, 3) Tide level, and 4) Modulus of elasticity.

The main objective is to assess the structural response of the lighthouse under ''wave 1'' loading by reproducing the in-situ accelerometer measurements using finite element simulation. The modeled wave by its 2 components the dynamic and the quasi-static must cause the same structural response parameters measured in-situ. Therefore, the aim mainly is to shed some light on slamming pressure magnitude, the impact area, the tide level, breaking types, and their effect on the dynamic response.

The level of tide is an important parameter to assess. The zone of load application is highly depended on this factor. Therefore, the 19-meter wave considered for this study is modeled with 2 tide levels as shown in figures 20 and 21. The first is +1.3 CD which was the tide level +1.3 m CD at the moment of breaking (12.7 m below the top level of the substructure). The second corresponds to the highest tide level which +8.2 m CD approximately 6 m below the top substructure. It is like shifting the same wave upward by 6.9 m to the maximum tide level.

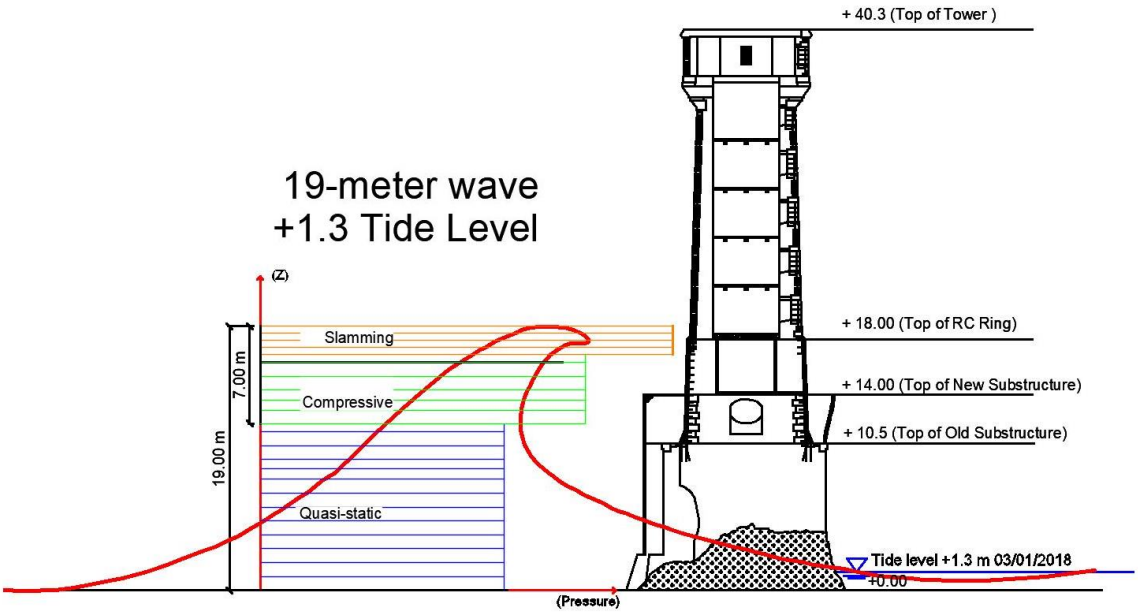

Figure 20:19-meter wave with 1.3-meter tide level

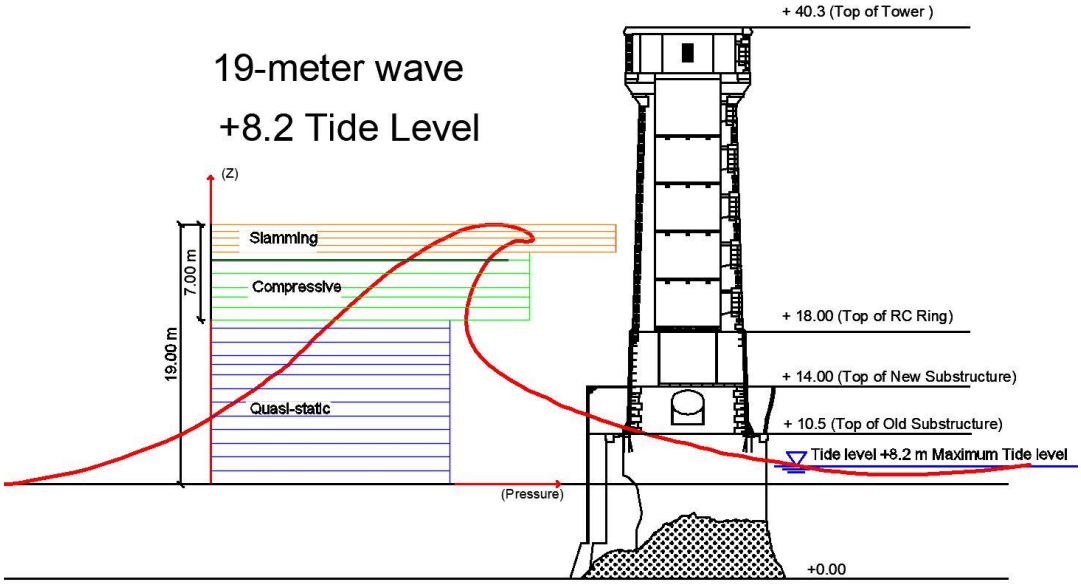

Figure 21:19-meter wave with +8.2 m tide level

Moreover, 3 different loads are applied to figure out the most likely pressure magnitude of wave 1. The first is with a maximum pressure of 230 kPa whereas the second and the third are with 300 kPa and 500 kPa respectively. The 3 different scenarios are modeled in one simulation as 3 consecutive waves with 4 seconds in-between which is an enough duration for damping in DIANA, figure 22.

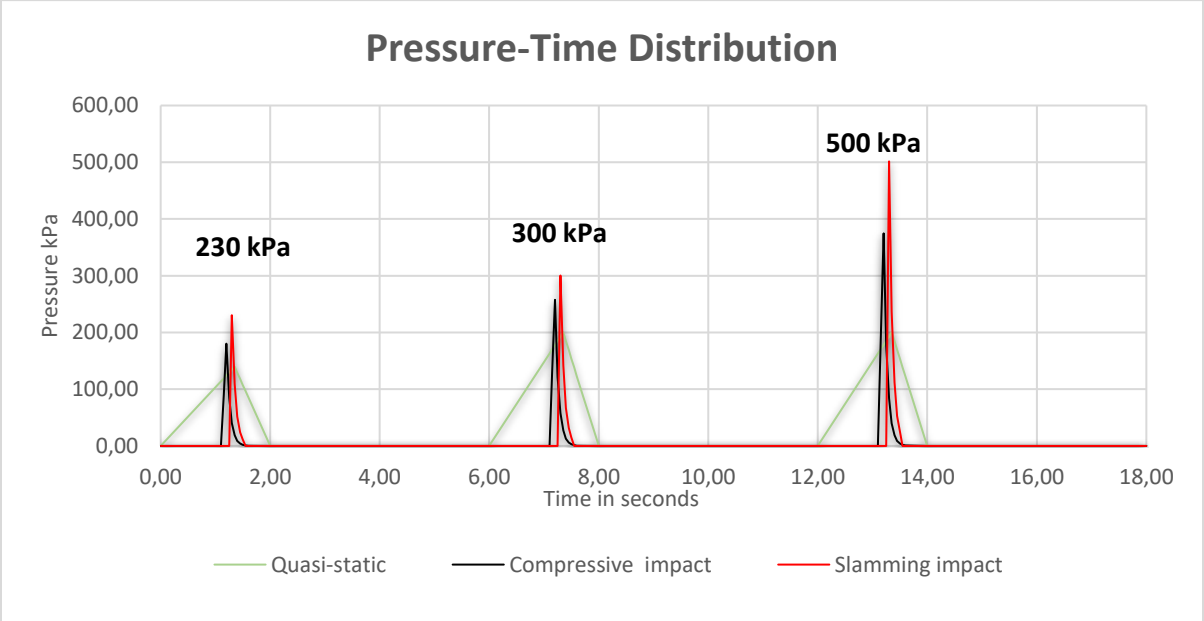

Figure 22:Pressure- Time distribution (3 cases: 230 kPa, 300 kPa, 500 kPa)

Assuming plunging breakers, the dynamic impact area for a 19-m wave is calculated as follows.

$$\text{Height of Impact area} = \lambda \times 0.8 \times H_b = 0.46 \times 0.8 \times 19 = 7 \text{ m}.$$

The 7-meter height is divided into 2 pressures blocks: The first is applied over a height of 2 or 3 meter which represent the slamming impact on top of the second block that represents the compressive impact. Thus, while respecting the impact area, the dynamic load is distributed over 2 areas. One is referred as slamming impact whereas the other is referred as compressive impact.

Finally, the analysis is performed with 2 modulus of elasticity 10 GPa and 15 GPa.

Figure 23 and 24 illustrate the horizontal and vertical distribution modeled in DIANA 10.5.

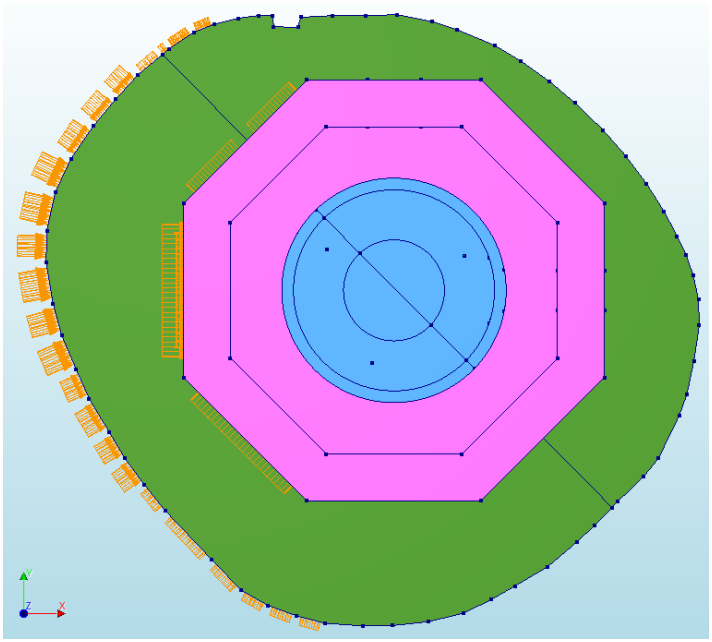

Figure 23:Top view, Horizontal distribution in DIANA

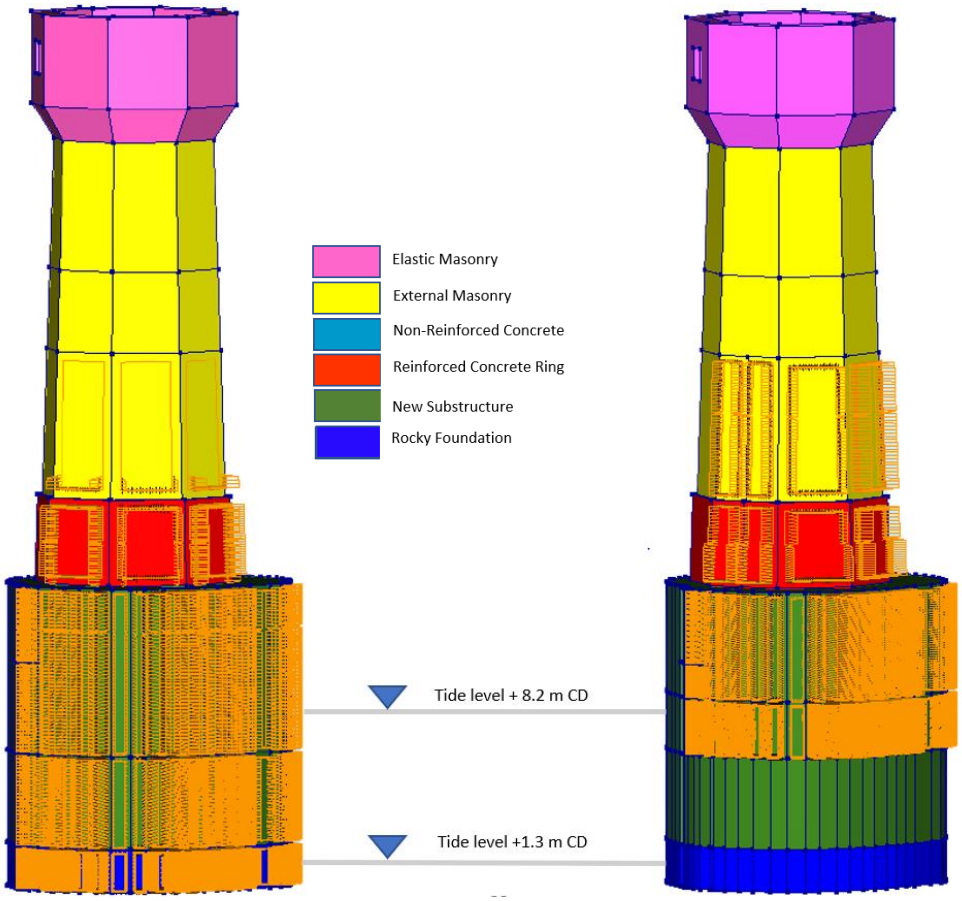

Figure 24:19-meter wave modeled in DIANA with a tide level of + 1.3 m CD and +8.2 m CD respectively

6 Model Calibration

6.1 Eigenfrequencies Calculations

This complex structure has different mode of vibration. A structural eigen-value analysis using DIANA 10.5 is performed and the first 9 natural frequencies of the lighthouse for both modulus of elasticity of 10 GPa and 15 GPa are summarized in the following table.

Table 3:Natural frequencies obtained with DIANA

Mode	ID in DIANA	Natural frequency (Hz) E= 10 GPa	Natural frequency (Hz) E= 15 GPa	Mode shape axis
1	1	3.15	3.81	X-axis
	2	3.32	3.91	Y-axis
2	3	11.18	13.23	Y-axis
	4	11.41	13.46	Y-axis
	5	11.81	13.9	X-axis
Axial	6	17.66	21.12	Axial (Z axis)
3	7	20.80	24.16	Y-axis
	8	21.07	24.45	X-axis
Torsional	9	25.31	30.91	Torsional

The 1st and 2nd natural frequencies correspond to **mode 1**. One is along the X direction and the other is along the y direction. Figure 25.

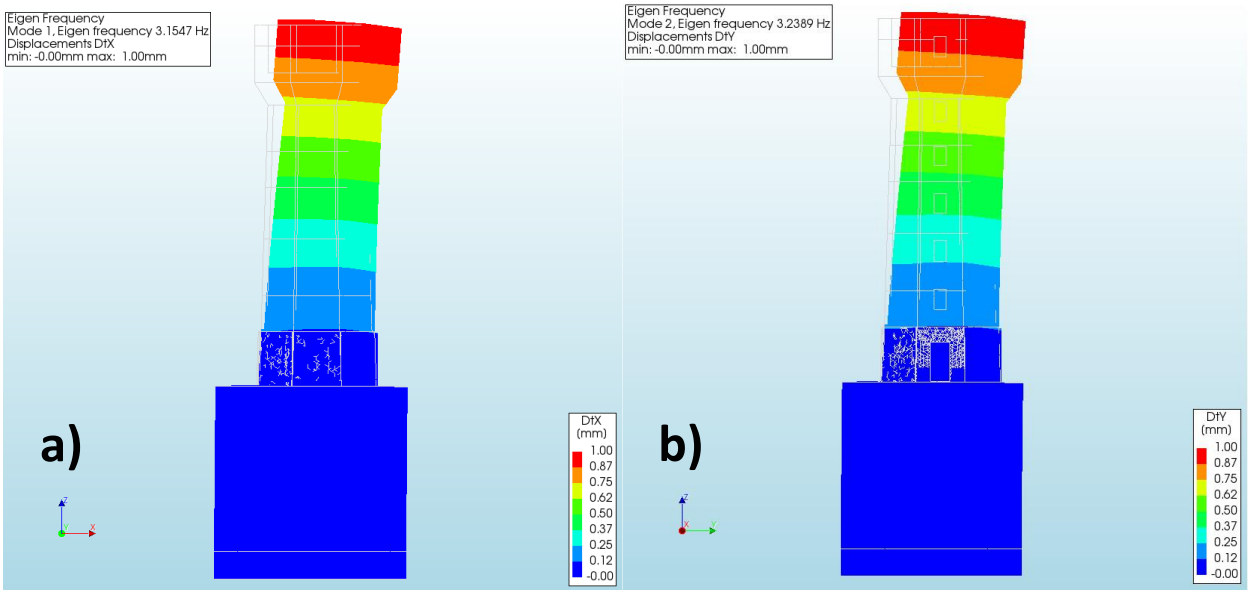

Figure 25: First Mode of vibration a) Along positive X, b) Along positive Y). E = 10 GPa

The 3rd, 4th, and 5th, natural frequencies correspond to **mode 2** shown in figure 26 a. The 3rd and the 4th natural frequencies are along Y and the 5th one is along X. Furthermore, the 7th and 8thnatural frequencies correspond to **mode 3** shown in figure 26 b. The 7th natural frequency is along Y whereas the 8th one is along X.

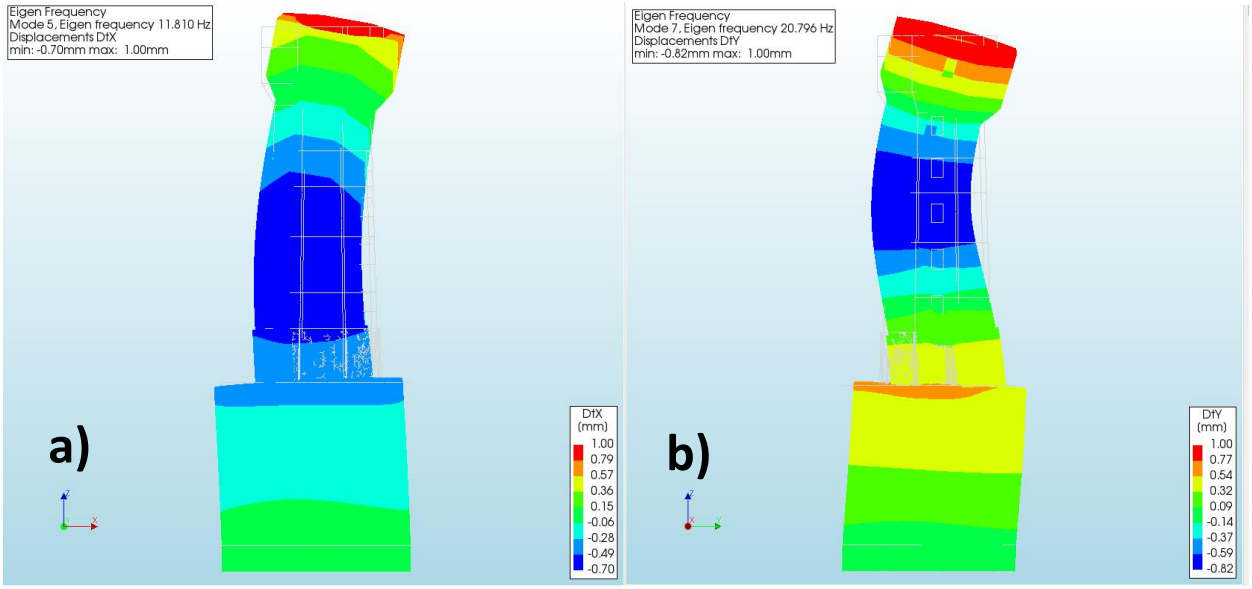

Figure 26:a)Second mode of vibration, b)3rd mode of vibration. E=10 GPa

The 5th natural frequency by DIANA correspond to the **axial mode** (along Z), whereas he 9th corresponds to the **torsional mode** shown in figure 27 a and b respectively.

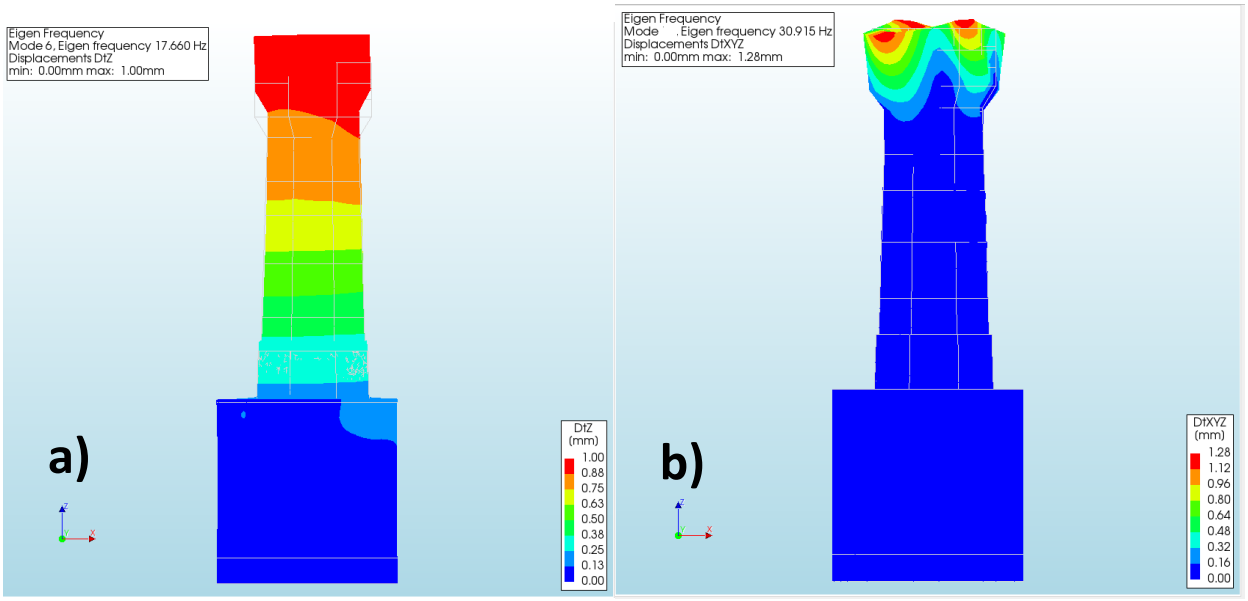

Figure 27: a) Axial mode (along Z), b) Torsional mode

6.2 Comparison with in-situ measurements

The first mode of natural vibration calculated by DIANA is compared with the results of ambient vibration at la Jument as well as with the eigen values calculated based on accelerometers measurements induced by wave 1 in January 2018.

[4] calculated the modulus of elasticity of the materials used in the construction of the lighthouse based on equation 9 given by SIA 178. It is approximated to be equal to 30 GPa [SIA 178] as an average value for the inner and outer skin of the lighthouse.

$$E = 1000 * \times f_{xd} \quad \textit{Equation 9 where } f_{xd} \textit{ is the compressive strength of masonry in MPa}$$

The modulus of elasticity assumed in this study represents the ''cracked'' state of the masonry. It is usually taken as 33% to 50% of the calculated modulus of elasticity according to Euro code 8.

The accelerometers data induced by the impact of wave 1 in winter 2018 were analyzed with a high pass Butterworth filter to determine the eigenfrequencies of the lighthouse. The spectral analysis by [3] revealed a first mode of 3.66 Hz for the majority of the accelerometers and 3.9 Hz for the remaining.

Moreover, [29] analyzed the ambient vibrations measured in calm weather by a seismometer Type GeoSIG GVB-316 in 2013. The results revealed a natural frequency of 3.88 Hz. These values are similar to the frequency 3.78 Hz for vibrations measurement recorded with an oscillograph in 1935 [4].

Consequently, the first mode calculated by DIANA which is 3.81 for a modulus of elasticity of 15 GPa is the closest to actual measurements. Thus, the model must be calibrated with a 15 GPa modulus of elasticity because it confirms all the previous arguments. However, the second mode (11.23 to 11.7 Hz) obtained by Denarié analysis of the accelerometers [3] is closer to second mode calculated by DIANA with a modulus of elasticity of 10 GPa. (11.18 to a 11.8 Hz). Thus, Ideally, a modulus of elasticity between 10 and 15 GPa is representative of the actual state of the lighthouse.

As for the structural response results presented in section 7, they are mainly based on 10 GPa modulus which was the first assumption accounting to a decrease in the stiffness due to repeated waves load impact over the lifetime of the structure. Other results with the 15 GPa assumption are presented as well.

6.3 History damage diagram

Questioning the effective modulus of elasticity of the lighthouse is essential. The aim was to produce a history damage diagram that describes the evolution of damages throughout the history of lighthouse. The idea would be to plot evolution of modulus of elasticity vs time. As damages increase in the structure, the modulus of elasticity will decrease as well as the natural frequency.

Ideally, this diagram would consist of applying the waves load of the main remarkable events (giant waves of 1916, 1927,) at each phase of reinforcements. The lighthouse would progressively be damaged after such huge loads and its stiffness would decrease. This decrease of stiffness would be captured at each phase of loading. However, performing eigenvalues analysis before and after applying the huge loads gives exactly the same eigenfrequencies in DIANA, for all modes even if cracks are initiated in the lighthouse model. A simple Fast Fourier transform is based on linearity of the materials and cannot mainly capture the slope of loading and unloading behavior.

To conclude, some laboratory experiments were already performed in Zurich [30] on walls using shaking table to capture the evolution of stiffness and plastic deformation with the increase in the damage state of the structure whereas no study with a simple FEM calculation have captured that. Therefore, some future improvement for the constitutive model as well as performing a wavelet analysis are recommended to give an indication about the decrease in natural frequencies due to damages caused by strong excitation and to get an idea about the decrease in modulus of elasticity.

6.4 Damping parameters

A typical damping ratio for concrete and masonry structures is between 0 and 20%. In this section, the damping characteristics are calculated based on the Rayleigh's method. 5% damping is calculated by [3] based on the decay of the accelerometer's measurements.

The damping is given by [31] as the following, equation 10:

$$|C|=a|M|+b|K| \quad \textit{Equation 10}$$

where C is the damping matrix that relates the mass matrix M and the stiffness matrix K. Coefficients a and b are the mass and stiffness Rayleigh damping constants respectively.

The damping ratio ζ_n for the nth mode of vibrations ω_n can be expressed as follows, equation 11.

$$\zeta_n = \frac{a}{2}\frac{1}{\omega_n} + \frac{b}{2}\omega_n \quad \textit{Equation 11}$$

Equation 11 can be expressed as well for two modes in a matrix form as in equation 12.

$$\begin{pmatrix}\zeta_0\\ \zeta_1\end{pmatrix} = \frac{1}{2}\begin{bmatrix}1/\omega_i & \omega_i\\ 1/\omega_j & \omega_j\end{bmatrix}\begin{pmatrix}a\\ b\end{pmatrix} \quad \textit{Equation 12}$$

In this study, the mass (a) and stiffness (b) Rayleigh damping constants are determined for the ith and jth mode with the same damping ratio of 5% which must be attained in all other modes that contributes significantly to the structural response. They are expressed in the following equations: $a = \zeta\frac{2\omega_i\omega_j}{\omega_i+\omega_j}$ and $b = \zeta\frac{2}{\omega_i+\omega_j}$ Equation 13 with $\omega = 2\pi f$

The mode 1 and 3 with (frequency of 3.85 Hz and 24.3 Hz respectively) are chosen to ensure a reasonable damping lower than 5% for all other mode. Usually, the natural frequency that corresponds to ω_j must be chosen based on the lowest peak of the frequency spectrum analysis which in fact is close to the 3rd mode in [3]. The constant a is equal to 2.088 and b is equal to 0.0006. It Is worth noting that [4] previously calculated those values a = 1.394 and b = 0.0007 based on the geometry of the lighthouses before the reinforcements in 1916.

Choosing a global damping for phased historical analysis is one of the limitations in DIANA since it is assigned to the materials which are the same before or after reinforcement. However, after the reinforcement, La Jument became stiffer with higher eigenfrequencies because the tower length was shortened by the elevation of the substructure. [4] used the damping characteristics of the structure before reinforcement and this underestimate the damping for the actual structure.

The following results in section 7 are based on damping characteristics of the old structure before reinforcement. This will not affect the maximal displacement caused by waves actions. However, it will slightly affect the decay of the acceleration.

7 Structural response parameters by FEM calculations

7.1 Overview

The main aim of this section is to reproduce by FEM analysis the accelerometers measurements from 3 January 2018 corresponding to wave 1 with a tide level of +1.3 m CD.

This study depends on 2 main parameters. The first parameter is the slamming impact pressure. 3 main pressure are assessed: 230 kPa, 300 kPa, and 500 kPa. For example, a scenario with a pressure magnitude less than 200 kPa is not strongly supported by theoretical hypothesis and therefore it is not considered. The second parameter is the portion of the impact area allocated for the slamming impact. Two scenarios are proposed regarding the slamming impact height ratio. The first considers a slamming height of 3 meters out of the 7 meters impact area and the other is 2 meters slamming height out of the 7 meters. Moreover, the effect of tide level on the structure is analyzed. The exact same 19-m wave is modeled with a tide level of +1.3 m as well as the highest astronomical tide level +8.2 CD corresponding to the assumption of Loraux [4]

Most of the results are given for modulus of elasticity of 10 GPa whereas the final simulation is performed using the 15 GPa modulus.

The different scenarios for this chapter are summarized in the following table:

Table 4: Different scenarios considered for the parametric study

19-m wave	Slamming Pressure [kPa]	Tide Level [m]	Modulus of Elasticity [GPa]	Slamming Height Ratio [m/m]
Section 7.2	500 **vs** 300 **vs** 230	+1.3m **vs** +8.2m	10	3/7
Section 7.3	230	+1.3m	10	3/7 **vs** 2/7
Section 7.4	230	+1.3m	10 **vs** 15	2/7

The main outputs of this section are structural response parameters ,acceleration and displacement ,at the position of the accelerometers deployed in the in-situ measurements. Three out of the four accelerometers installed can be considered for comparison with FEM analysis, in particular accelerometer 3 which is at position +38.75 m, Appendix 1. Accelerometer 4 is not considered for this study since it was installed on the lantern which is not modeled in this study. Moreover, it is installed on a metallic frame with a damping ratio of 9% [3] and not on masonry. Thus, its data is not representative for the wave impact analysis of the tower.

The positive direction for acceleration and displacement is along the direction of wave impact. (55 ° Azimuth) in all what follows.

7.2 Effect of tide level and Pressure magnitude

The structural responses parameters calculated by FEM at the level of accelerometer 3 at +38.75 m are the following.

Figures 28 and 29 illustrate the accelerations for 3 pressures at a level +38.75 m with slamming height 3 m out of 7 m and modulus of elasticity of 10 GPa.

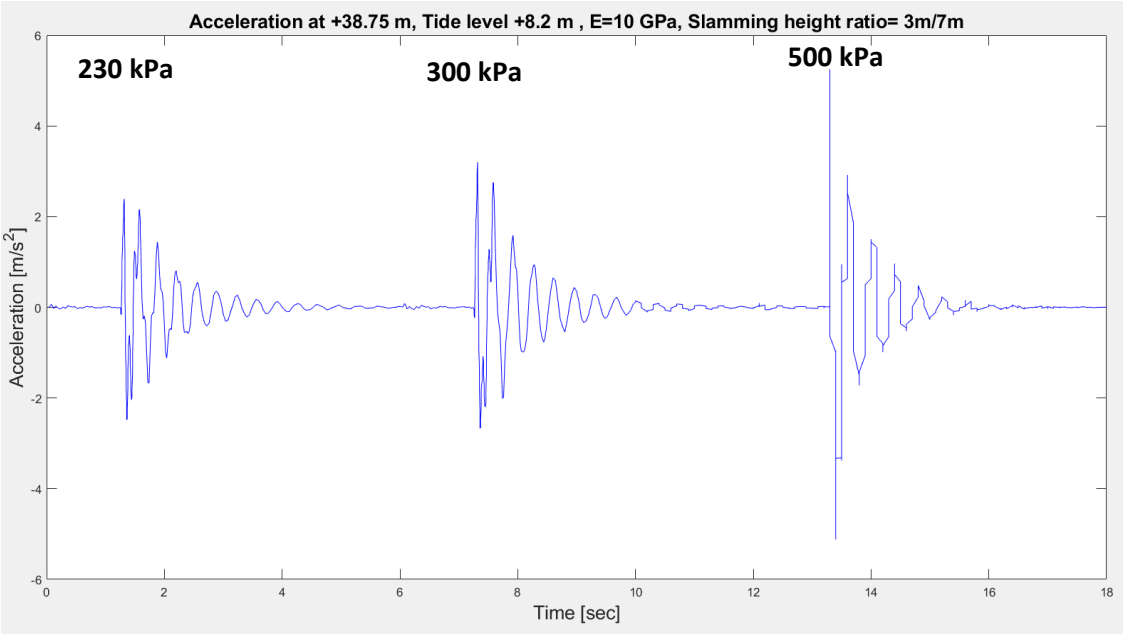

*Figure 28: Acceleration (m/s^2) at +38.75 m, Tide level **+8.2 m**, E = 10 GPa, Slamming height is 3m*

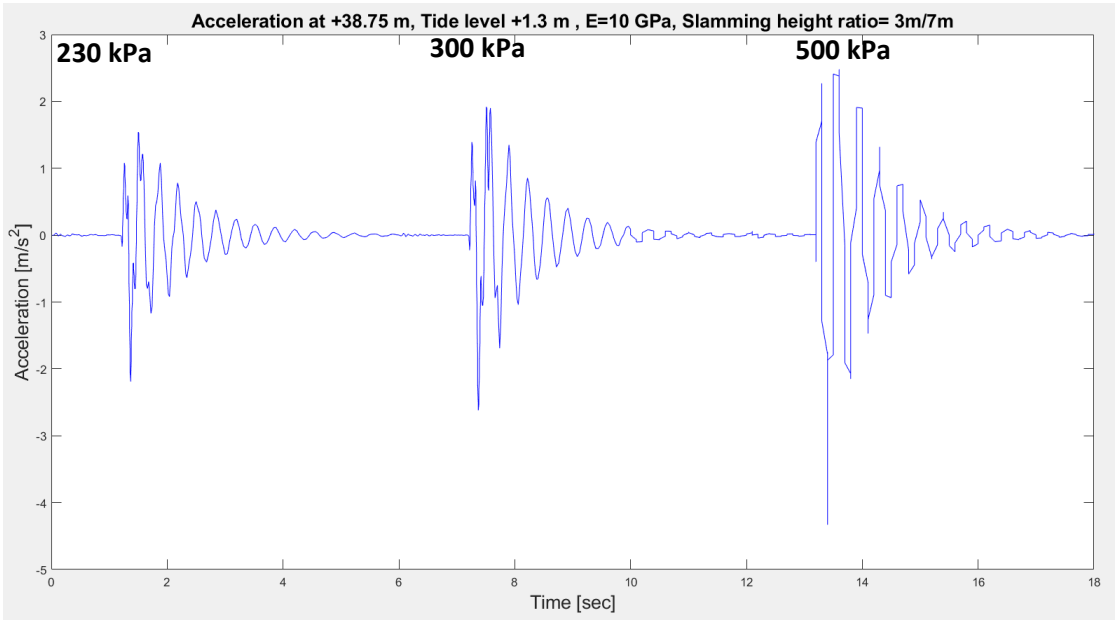

*Figure 29:Acceleration (m/s^2) at +38.75 m, Tide level +**1.3 m**, E = 10 GPa. Slamming height is 3m*

Figures 30 and 31 illustrate the displacements for 3 pressures magnitude at a level +38.75 m CD with slamming height 3 m out of 7 m and modulus of elasticity of 10 GPa.

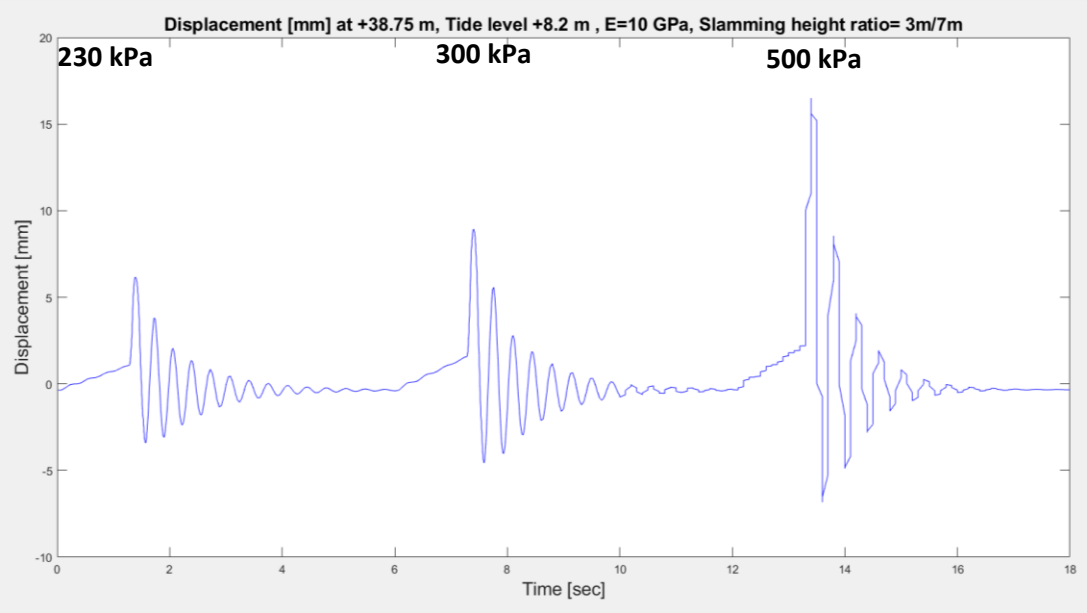

*Figure 30: Displacement [mm] at +38.75 m, Tide level **+8.2** m, E = 10 GPa. Slamming height is 3m*

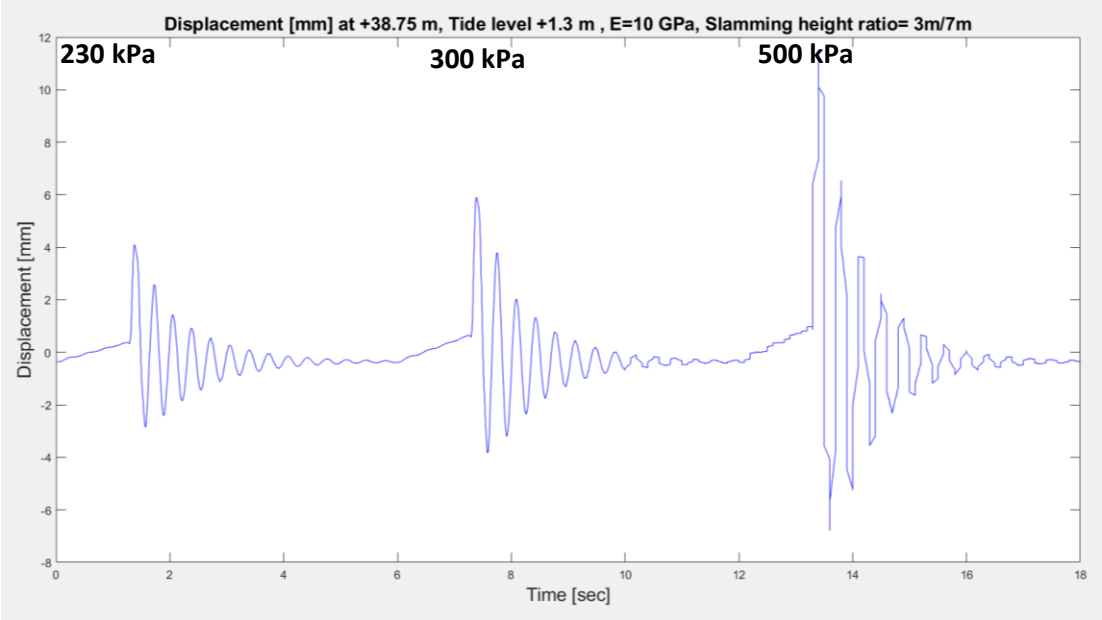

*Figure 31:Displacement [mm] at +38.75 m, Tide level **+1.3** m, E = 10 GPa. Slamming height is 3m*

As the pressure magnitude increases, the acceleration and displacement increase. Moreover, the increase in tide level creates higher displacement and acceleration. This result is reasonable and as expected.

Table 5 summarizes the previous results corresponding to 3 different pressures magnitude as well as 2 different tide level +1.3 m and +8.2 m. The modulus of elasticity considered is 10 GPa and the height of the slamming impact is 3m out of 7 m.

Table 5:Displacements and Accelerations range as function of tide level and pressure magnitude at level +38.75 CD Chart Datum

19-meter wave							Actual In-situ Measurements
Slamming Height Ratio (m/m)	3/7						Unknown
E (GPa)	10						Unknown
Tide Level (m – above CD)	**+8.2**			**+1.3**			**+1.3**
Slamming Pressure (kPa)	**500**	**300**	**230**	**500**	**300**	**230**	Unknown
Displacement (mm)	+16.5 -6.8	+9.0 -4.6	+6.2 -3.4	+11.5 -6.5	+5.9 -3.8	+4.1 -2.9	+1.1 -1.9
Acceleration (m/s^2)	+5.3 -5.0	+3.2 -2.7	+2.4 -2.5	+2.4 -4.3	+1.8 -2.5	+1.5 -2.1	+0.9 -1.1

Firstly, the results are compared between the 2 different tide levels. For the different pressure magnitudes, the same trend is observed for displacement going from +8.2 m tide level to +1.3 m tide level. For the highest tide level +8.2 m, the displacements are 50% higher in the direction of load application (Positive displacement) whereas they are only 5 to 20 % higher in the inverse direction. As for the acceleration, there is an observed decrease with the decrease of tide level as well as with the decrease in slamming pressure but with a less clear trend. Going from +8.2 m tide level to +1.3 tide level, the acceleration dropped by 50% for the 500 kPa and by 40% for the 230 and 300 kPa in the positive direction. However, in the inverse direction of loading, a slight decrease is observed 9%to 15%. Thus, the decrease in acceleration is notable in the direction of the wave impact whereas in the inverse direction, the acceleration is slightly changed.

Therefore, the tide level is an important factor to consider, and the results are reasonable since the zone of load application is approximately 7 meters higher.

Secondly, the results clearly show that the most likely slamming pressure for wave 1 is 230 GPa which gives displacement and acceleration closer to the real measurements. This pressure is actually close to values calculated by [21]. The wave considered was a 20-meter wave with a 11 seconds period whereas wave 1 is a 19-meter wave with 13 seconds period.

7.3 Slamming height effect

According to the information gathered from literature for this study, the impact height is clearly defined based on the breaking type. In this case study, 7 meter is the impact height for a 19-meter wave. However, there is no rule that specifies: (1) the portion of this impact that corresponds to the slamming pressure, and (2) which portion corresponds to the compressive impact. Two different scenarios were considered for this study. The Slamming height for the first is 3 meters as previously shown in section 7.2 whereas the slamming height for the second is 2 meter out of 7 meters.

Structural responses parameters calculated by FEM at the level of accelerometer 3 at +38.75 m are displayed as the following. 2 slamming height ratios are assessed with the same modulus of elasticity of 10 GPa and same tide level +1.3 m CD.

Figures 32 and 33 illustrate the acceleration and displacement respectively for a slamming height of 2 m out of 7 m with a modulus of elasticity of 10 GPa and a tide level of +1.3 m. The results for the same conditions but with the slamming height of 3 m out of 7 m are already displayed in figures 29 and 31.

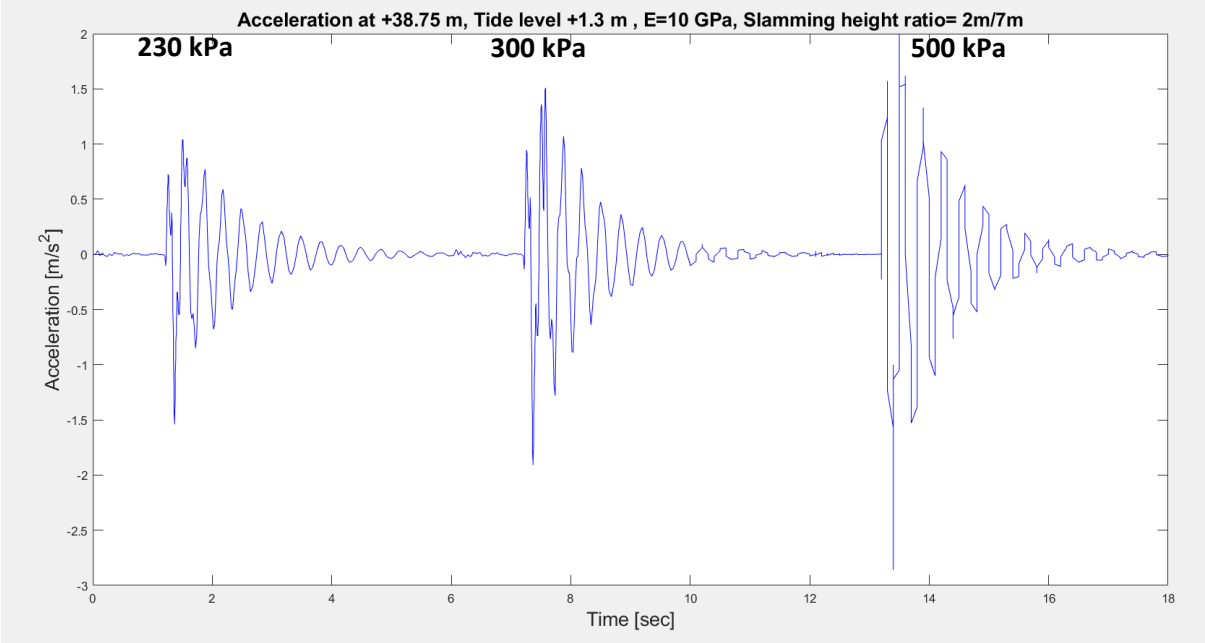

*Figure 32: Acceleration (m/s^2) at +38.75 m, Tide level +1.3 m, E = 10 GPa. Slamming height is **2m***

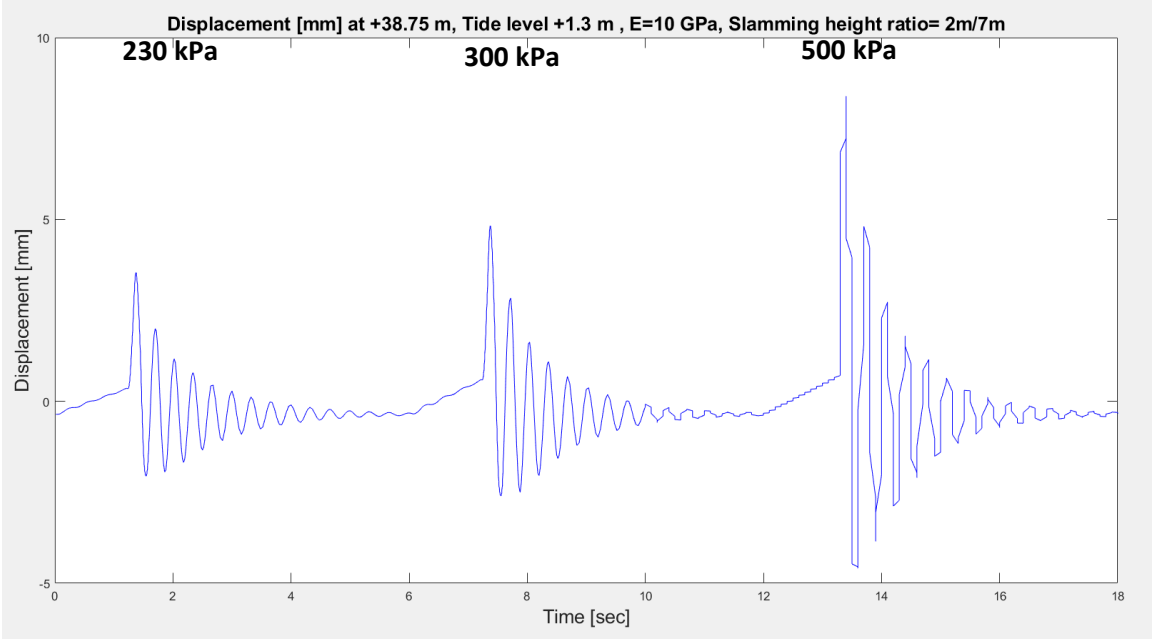

*Figure 33:Displacement (mm) at +38.75 m, Tide level +1.3 m, E = 10 GPa. Slamming height is **2m***

As the slamming height ratio decreased from 3m/7m to 2m/7m, the displacement decreased by approximately 30% in the positive direction of wave loading and 15% in the inverse direction whereas the accelerations decrease by 30% in both directions.

Table 6 summarizes the influence of the slamming height ratio for the most likely pressure magnitude of 230 kPa considering the same tide level +1.3 m and modulus of elasticity 10 GPa.

Table 6:Displacements and accelerations range as function of slamming area at level +38.75 CD

19-meter wave			Actual In-situ Measurements
Tide Level (m - above CD)	+1.3		+1.3
E (GPa)	10		Unknown
Slamming Pressure (kPa)	230		Unknown
Slamming Height Ratio (m/m)	**3**/7	**2**/7	Unknown
Displacement (mm)	+4.1 -2.9	+3.5 -2.0	+1.2 -1.9
Acceleration (m/s^2)	+1.5 -2.1	+1 -1.5	+0.9 -1.1

Two meters slamming pressure height with 230 kPa magnitude gives a result closer to the actual measurements of 3 January 2018. In fact, the displacement in the positive directions is almost the triple of the actual measurements whereas in the negative direction it is almost the same (-2 mm vs -1.9 mm).

This factor presents a high level of importance while performing FEM calculation and must be confirmed by laboratory experiments as well as in-situ experiments by integrating pressure transducers in the lighthouse facing the waves direction.

Therefore, for the scope of this study, the most likely slamming pressure is 230 kPa which is confirmed by [21] for a similar wave. The height of the area where the slamming pressure is concentrated over the dynamic impact area is evaluated. A slight decrease of 30% is observed for acceleration and displacement going from 3 meters slamming height to 2 meters slamming height.

7.4 Modulus of elasticity effect

As discussed in section 6.2, the most likely global apparent modulus of elasticity of La Jument is between 10 and 15 GPa. The 15 GPa gives a first mode of natural frequency closer to the ambient vibrations measurements as well as the spectral response analysis performed by [3] for the accelerometers' measurements on 3 January 2018. The 10 GPa represents the lower bound of the effective modulus of elasticity of cracked sections (33% of the compressive strength 30 GPa). Furthermore, the second mode calculated by DIANA is closer to the second mode determined by the spectral response analysis [3].

Figures 34 and 35 illustrate the acceleration and displacement respectively for a 19-meter wave with a tide level of 1.3 m and a slamming height ratio of 2m/7m considering a modulus of 15 GPa at the level of accelerometer 3 at +38.75 m. They are summarized in table 7 as well.

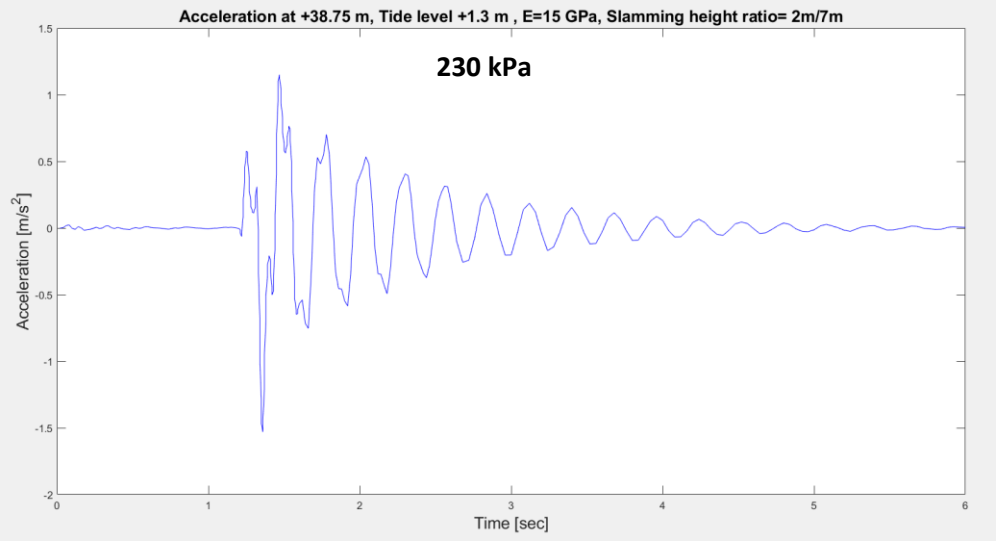

*Figure 34:Acceleration (m/s2) at +38.75 m, Tide level +1.3 m, E = **15GPa**. Slamming height is 2m*

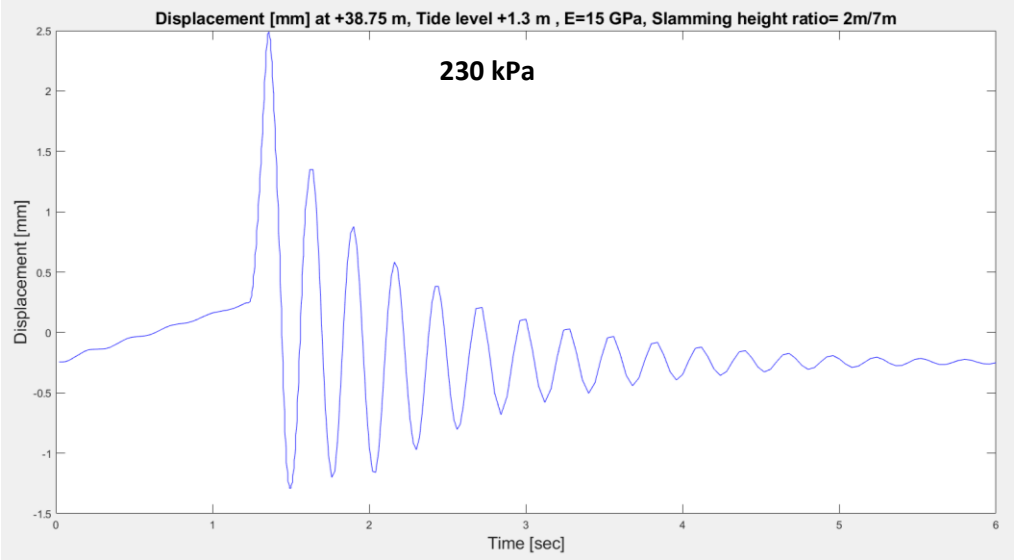

*Figure 35:Displacement (mm) at +38.75 m, Tide level +1.3 m, **E = 15 GPa**. Slamming height is 2m*

Table 7:Displacements and Accelerations at level +38.75 m CD as function of global modulus of elasticity of the structure.

	19-meter wave		Actual In-situ Measurements
Tide Level (m – above CD)	+1.3		+1.3
Slamming Pressure (kPa)	230		Unknown
Slamming height Ratio (m/m)	2/7		Unknown
E (GPa)	**10**	**15**	Unknown
Displacement (mm)	+3.5 -2.0	+2.5 -1.3	+1.2 -1.9
Acceleration (m/s^2)	+1.0 -1.5	+1.1 -1.6	+0.9 -1.1

As discussed earlier, the modulus of elasticity that represents the cracked state of the structure is approximately 15 GPa. Calculation by FEM shows that the acceleration and displacements for a 15 GPa modulus are closer to the actual measurement than for a 10 GPa.

The increase of modulus of elasticity decreases the displacement by 30 % in the direction of the incoming wave as well as the inverse direction. However, the acceleration is slightly higher for the modulus of 15 GPa ($+0.05$ m/s2) which is considered negligible. Positive displacements and accelerations are in the direction of Incoming wave: + 55° Azimuth. Negative displacements and accelerations are in the inverse direction: 235° Azimuth

To sum up, for both modulus of elasticity considered for this study, the accelerations and displacement calculated by DIANA are comparable to the in-situ measurement. Future researches can build on the assumption taken in this study. Ideally, a modulus of elasticity between 10 GPa and 15 GPa is the most representative of the actual cracked state. Methods to determine this parameter are mentioned in section 8.5.

7.5 Comparison along the height of the lighthouse

The accelerations and displacements based on FEM calculation for the model with 230 kPa slamming pressure, modulus of elasticity 15 GPa, +1.3-meter level tide, and 2 meters of slamming pressure height are compared with the actual in-situ measurements obtained from [3] in table 8. The vertical positions of accelerometers a1, a2, and a3 [appendix 1] are +20.6 m, +31.1 m, and +38.75 m CD respectively. The positive acceleration and displacement are along the wave direction (+55° azimuth).

Table 8: Accelerations and Displacements along the height of the lighthouse; Pressure 230 kPa, E=15 GPa, Slamming height ratio 2m/7m

19-m wave	**Level of accelerometer a1 +20.63m CD**		**Level of accelerometer a2 +31.1 m CD**		**Level of accelerometer a3 +38.75 m CD**	
	DIANA Calculations	Actual measurements	DIANA Calculations	Actual measurements	DIANA Calculations	Actual measurements
Displacement (mm)	+0.9 -0.3	+0.3 -0.6	+1.6 -0.8	+1.0 -1.1	+2.5 -1.3	+1.2 -1.9
Acceleration (m/s^2)	+0.5 -0.7	+0.4 -0.6	+0.7 -0.7	+0.8 -0.9	+1.1 -1.6	+0.9 -1.1

The reasonable result expected for this section is that the acceleration and displacement increase along the height of the lighthouse. This is clearly presented in table 8.

The FEM calculations are comparable to the actual measurements in January 2018 for the 3 accelerometers. To illustrate that visually, the results of accelerometer 3 are considered for superposition with experimental results in the following section.

7.6 Superposition of FEM calculation and actual measurements

In this section, the similarities and discrepancies between experimental results and FEM calculations are illustrated by superposing them in the same plot.

7.6.1 Accelerations and displacement superposition

The starting point of the X axis corresponds to the time 9:42:07 UTC on 3 January 2018 approximately 0.5 seconds before breaking. The experimental data was filtered with a high pass filter order 3 and a low pass filter order 2 by [3]. [3] further integrated the accelerations results twice to get the displacement. The data used in the plot corresponds to accelerometer 3 at +38.75 m in the positive direction described earlier (55° Azimuth) which is referred in [3] as ''aZ3'' shown in figure 36.

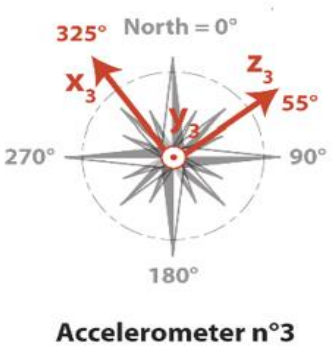

Figure 36: Accelerometer 3 orientation at +38.75 m as described in [3]

As for the calculated acceleration and displacement by DIANA, the first 0.5 seconds were not considered for the superposition. This is because the time range of the experimental data is 4.5 seconds. In fact, the first 1.1 seconds in DIANA corresponds only to a gradual increase in the quasi-static component which can be neglected in future optimization or can be shortened. Furthermore, the last 1 second is not considered as well for the superposed plots, figure 37.

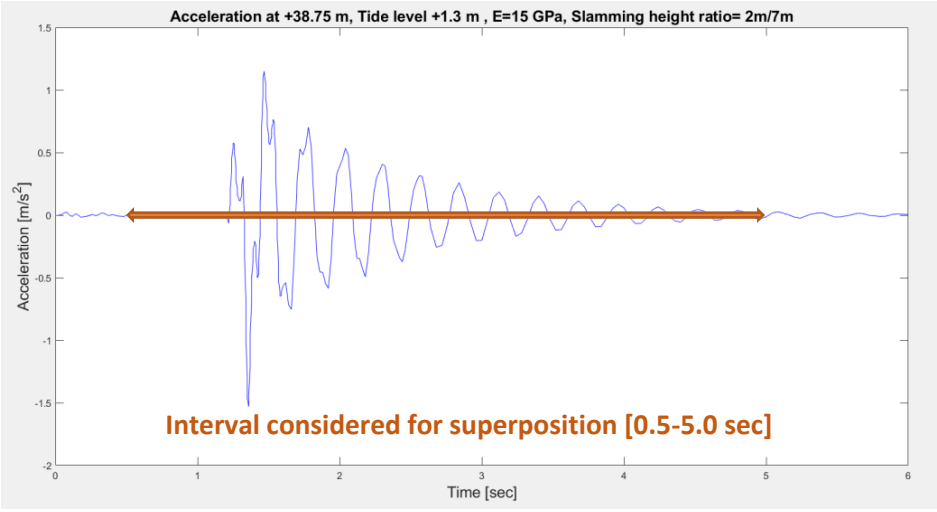

Figure 37: DIANA results considered for superposition

The scenario considered for superposition is mainly the closest to the actual measurements. It includes the combination of 2 meters slamming pressure height with 230 kPa magnitude and 15 GPa modulus of elasticity for the 1.3 m tide level.

The following plots, figure 38 and 39, illustrate the acceleration and displacement obtained from FEM calculations and the actual measurements at level +38.75 m CD.

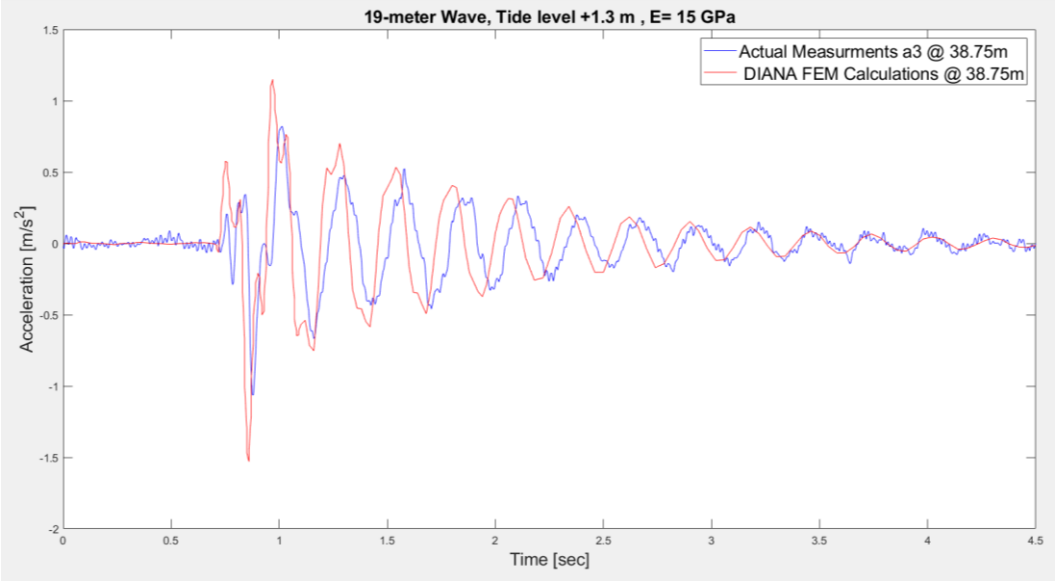

Figure 38: Superposed plot of the acceleration at +38.75 m (Measurement data by [3] vs FEM calculations)

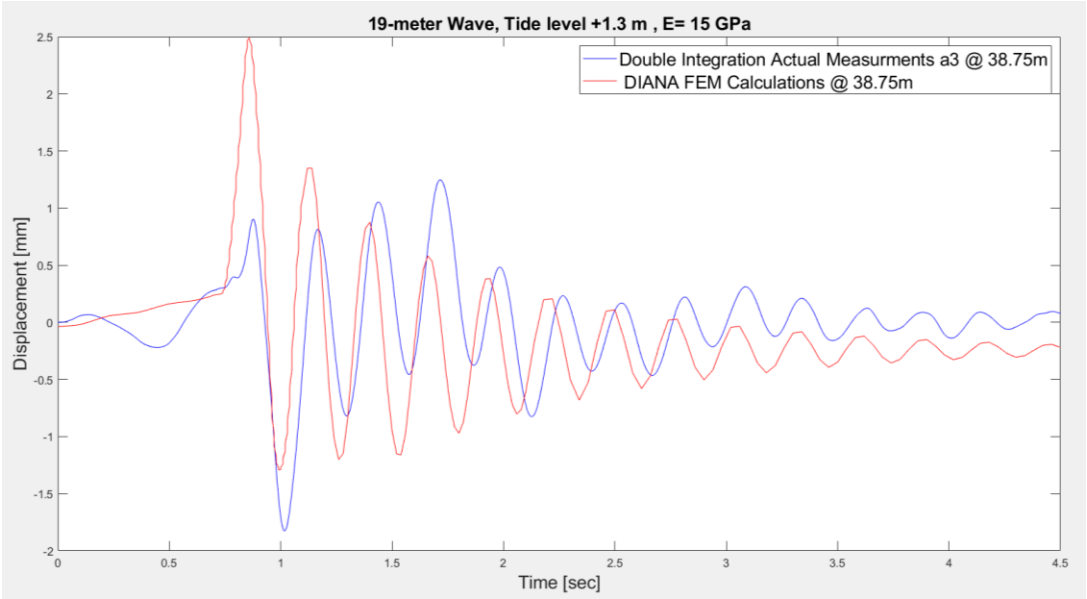

Figure 39:Superposed plot of the displacement at +38.75 m (Measurements data integrated twice by [3] vs FEM calculation)

The FE model was able to predict the accelerations measurements accurately. A perfect match can be seen all over the considered interval. As for the maximum acceleration, the FEM calculations overestimates the actual measurement by 30% approximately but it establishes a very clear trend.

However, the superposed plot of displacement presents some discrepancy between the actual measurements and the FEM calculations. The displacement prediction of the FE model is double the actual measurements in the positive direction whereas it is 30 % less in the inverse direction. There are number of possible reasons. The most important explanation is that the direction of wave is assumed to hit the tower perpendicularly on face 5 along the door's axis 55° azimuth to simplify its modeling in DIANA. However, it was hitting on the corner between 4 and 5 [3] and this could explain the larger displacement along the door's axis, figure 40. Another potential reason is that the top of the wave is modeled at level +19 m whereas according to the photographical documentation, the wave was hitting the top of the reinforced concrete ring approximately at +18 m or +18.2 m. Moreover, when the acceleration is almost null, the quasi linear ascending in displacement prior to the oscillation is likely to be an artefact of a double integration with non-zero constant. Thus, the displacement calculated by DIANA are likely to be overestimated.

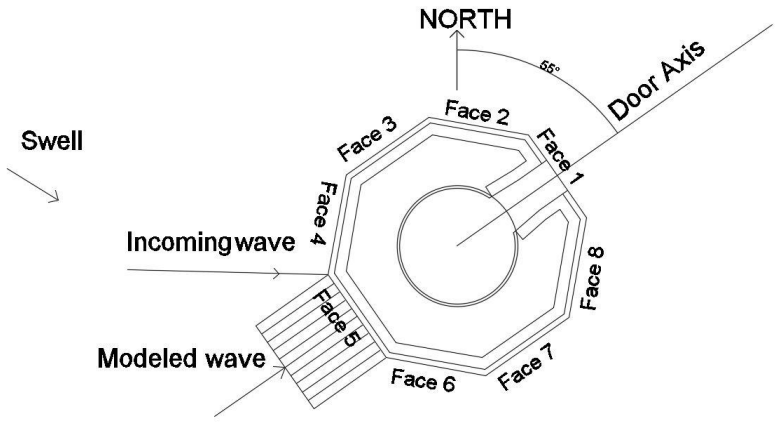

Figure 40:Modeled wave direction vs incoming wave

Ideally, the FEM calculations must give less displacement since the lighthouse is modeled monolithically which is not the actual state of the lighthouse undergone different reinforcement throughout the history. Separation between the tower and the base of 20 mm illustrated in section 8.2 gives more flexibility of the lighthouse where it can oscillate without restrictions.

Last but not least, the oscillation period (duration between 2 maximum values) for the acceleration and the displacement is almost the same for the experimental results and FEM calculation 0.28 sec and 0.26 sec respectively. This 0.02 second is due to the global damping characteristics assumed in section 6.4 for the old structure before the reinforcement.

7.6.2 Splash Vibration

[3] further described 2 main events. One starts after around 0.7 seconds on the dataset illustrated the superimposed plots in 7.6.1.

The second event starts at T= 1.7 seconds and is captured by the accelerometer in the direction perpendicular to waves direction (aX3 figure 36). Unfortunately, this is not captured by the DIANA calculations at T = 1.7 s as illustrated in figure 41. According to measurements obtained by [11], some strong oscillations were captured up to 1 to 2 seconds after the maximum pressure peak due to the resonance effect of cylinders. This could be one explanation of what happened in reality.

[2] mentioned that the water of the splash reached the top level of the masonry where the stereo video cameras were installed. A fast flow towards the crest can be associated with the onset of a secondary jet just below the main crest. Thus, the splash vibrations could be explained by a secondary effect of water impact on the upper part of the lighthouse. This can be modeled in future optimization as an impulse hitting the top of the lighthouse. However, many uncertainties remain for such a scenario.

The duration between the 2 events or in other word the duration of splash to reach the upper level of the lighthouse is 1.7-0.7= 1 second. This is confirmed by the time frame between 2 consecutives photographical documentations [3].

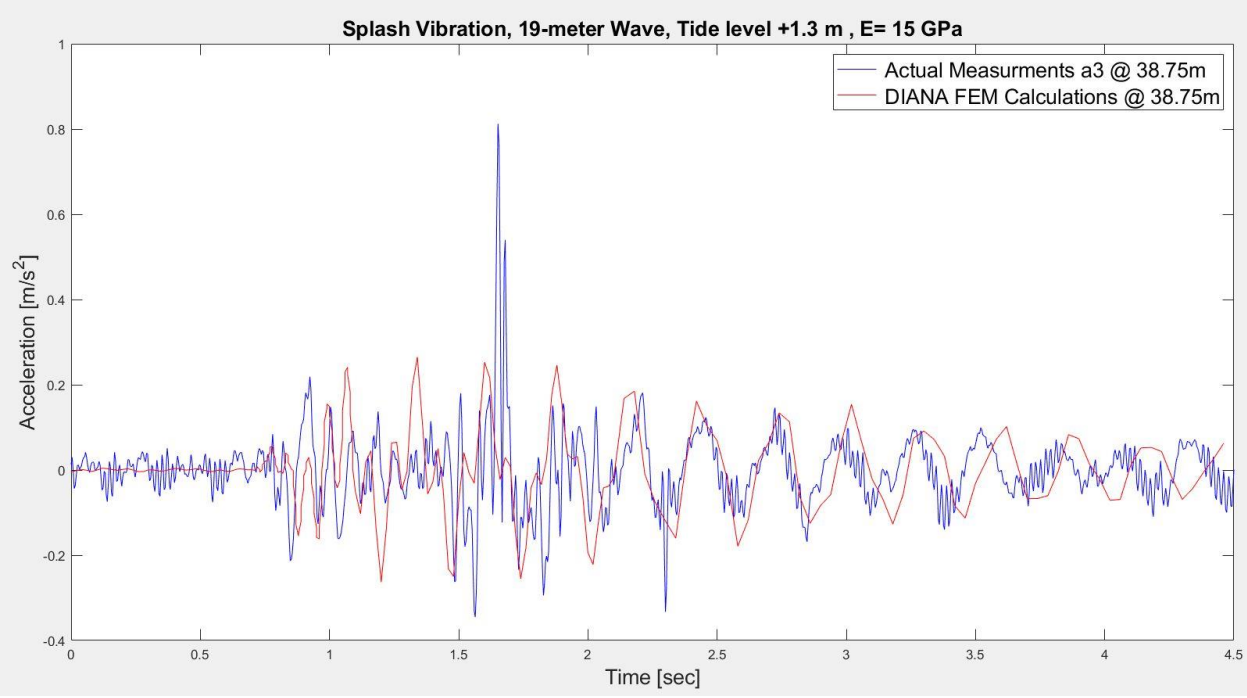

Figure 41: Splash Vibrations in the direction perpendicular to wave action (325° $Azimuth$)

7.7 Discussion and outlook

One of the main assumptions needed for the scope of this study was modeling the lighthouse monolithically which is not the case in reality. The structure has undergone different reinforcement as previously discussed (doubts about perfect bond between the current top part of the base and the tower) as well as has several cracks separating the concrete ring and the substructure. This is presented in section 8.2. This crack could be modeled as an interface separating the tower and the base, with contact mechanics. Their effect can be studied on the structural response of the tower. The connection of the old base and the rocky foundation as well as the connection between the tower and old base are questionable. The tower is not completely clamped along the height of the base.

The prestressing anchors are modeled in DIANA but there is some missing information about how they were installed back in 1934 in particular their anchoring with the rocky foundation. The functionality of these anchors is questionable. They might be corroded after 86 years of exposure to a very salty and aggressive environment. Since the steel lantern is not modeled, it can be represented by a pressure on the top equivalent to its weight. The cables and the top pressure equivalent to the lantern's weight were simulated in DIANA in this version. Their effect on the horizontal displacement and acceleration was null. However, they decreased vertical displacement by 1 mm which is negligible value as well.

The global damping mentioned in 6.4 is a limitation in DIANA to perform a historical assessment of the lighthouse. The value used in DIANA corresponds either to the structure before reinforcement or after reinforcement. This is not a major problem; however, it affects slightly the decay of the structural response.

8 Concept of maintenance

8.1 Motivation and open questions

Preserving and protecting “La Jument” is of great importance, given the key role it has played in facilitating strategic navigation over the years as well as the role it has played more recently in a better understanding of the non-linear characteristics of extreme waves event like in [2-3].

Wave impacts have different effects on the lighthouse other than the significant impact pressure. The water can penetrate the cracks at the top of the base. The water entering the cracks creates pressure that tends to cause spalling as well as to decrease the ultimate tensile strength and the stiffness. Masonry’s edges spalling is caused by alternating efforts of extension and compression. Moreover, some stones can travel with the waves which can cause damages when hitting the structure. Some stones were observed at the top of the base’s platform. The repeated waves impact on the tower create fatigue of the structure and can lead to serious problems in the future.

In-situ measurements significantly help in confirming the structure safety, validating numerical computation assumptions, and removing uncertainties about the lighthouse behavior under extreme waves loading. The previous measurement campaign at la Jument helped to some extent understanding characteristics of waves during winter storms. Furthermore, there are lots of uncertainties concerning the geometrical shape and state of the lighthouse such as cavities, cracks, heterogeneity in layers, texture, and thickness.

La Jument must be reinforced against such actions in particular preventing water from entering the existing cracks. In section 8.3, an intervention method is proposed.

Thus, other measurement campaigns are still necessary for monitoring purposes, and they must be extended for a longer period. The objective of section 8.4 is to propose waves pressure magnitude measurements campaign as well as to highlight methods to assess geometrical features and materials characteristics of La Jument.

8.2 Current conditions

La Jument lighthouse has survived 111 years of ocean storms with numerous extreme waves loading. In this section, the visual inspection is illustrated by means of photographical documentations [32-33].

Cracks were initiated to separate the new base and the concrete ring after the storm of 23 December 1927 which had the same intensity as the storm of 1916. The concrete ring base separation is along 3 different faces 4, 6 and 7. As for face 4, the separation is 10 mm whereas the critical separation is for face 6 and 7 with a 20 mm opening that goes up to 3 meters deep shown in figure 42. Thus, the tower is not completely clamped along the height of the base.

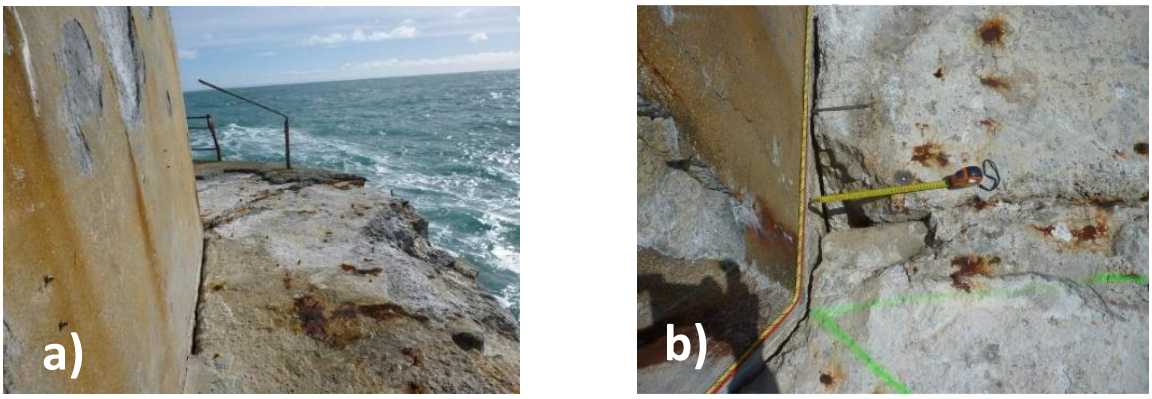

Figure 42: a) RC Ring and New base connection's separation; b) 20 mm crack with 3 m of depth [32]

Concrete spalling of the upper part of the base in the south direction (below Face 6) happened after a severe storm in 2014. Dry shotcrete was applied in 2015, figure 43.

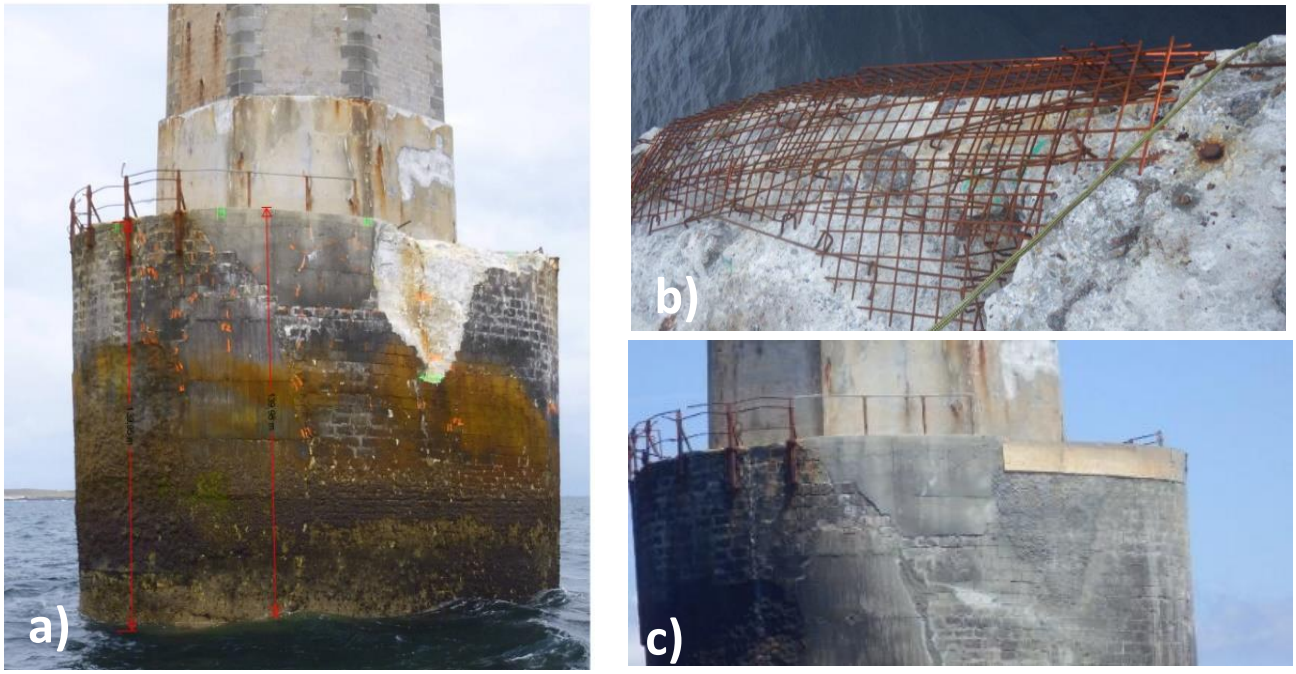

Figure 43: a) Concrete spalling after a severe storm in 2014[32]; b) & c) Shotcrete applied for reinforcement. [33]

As illustrated in figure 44, the rust is clearly visible on the reinforced concrete ring in particular the faces impacted by waves loading (Face 4, 5, and 6). This is due to the corrosion of reinforcements steel bars caused by the exposure to the severe salty environment. Furthermore, the main reason of cracks, delamination and spalling of the reinforced concrete ring are corrosion of steel bars and local wave actions.

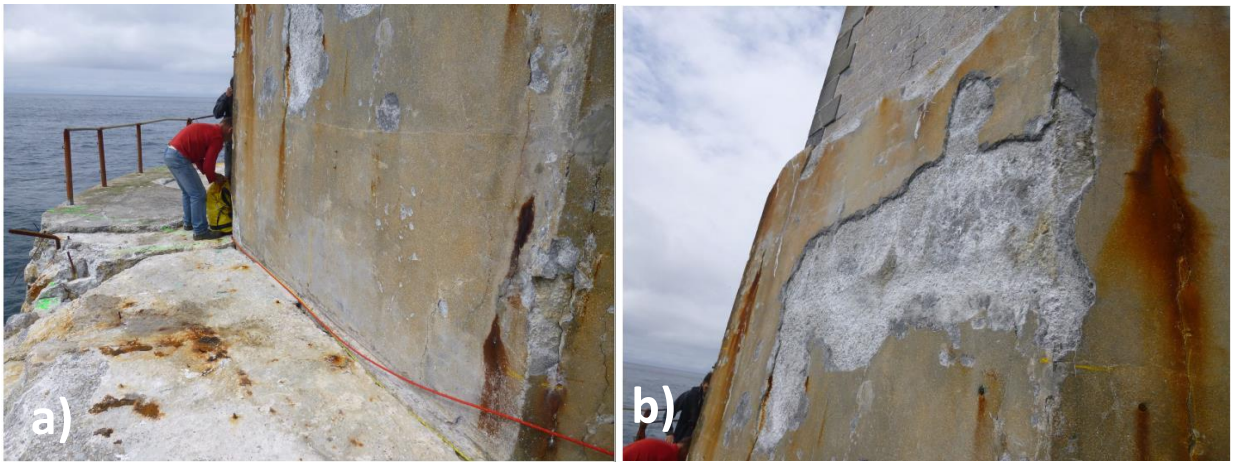

Figure 44: Damages of the concrete ring: a) Visible rust, b) Concrete delamination [32]

Moreover, a small separation ($\cong 5\ mm$) exists between the top of the concrete ring and the tower which was after closed by foam material to prevent water from entering, figure 45.

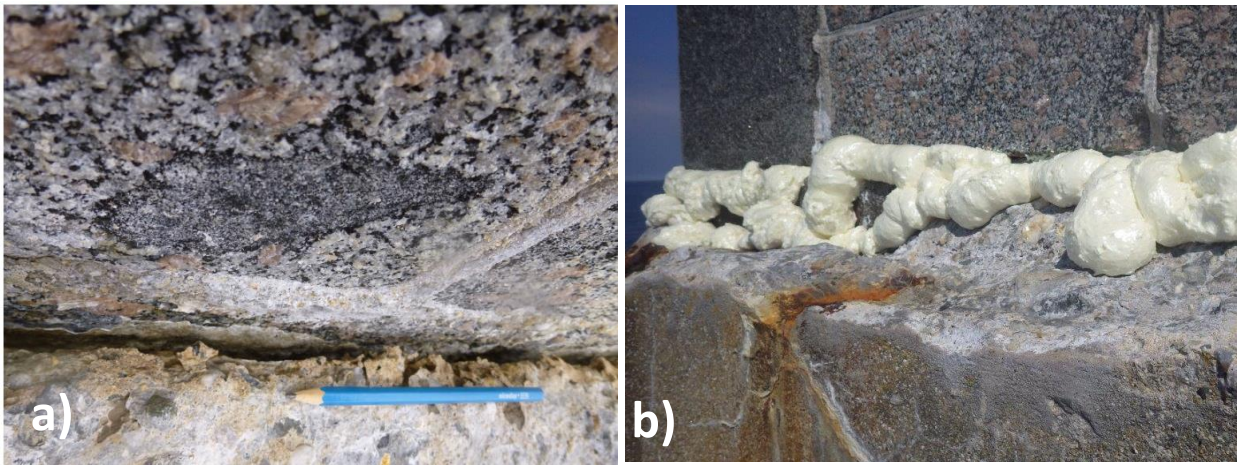

Figure 45: a) Concrete ring and tower separation [32]; b) Foam applied to prevent water [33]

Finally, numerous radial cracks can be seen on the platform which is the upper level of the base, as illustrated in figure 46.

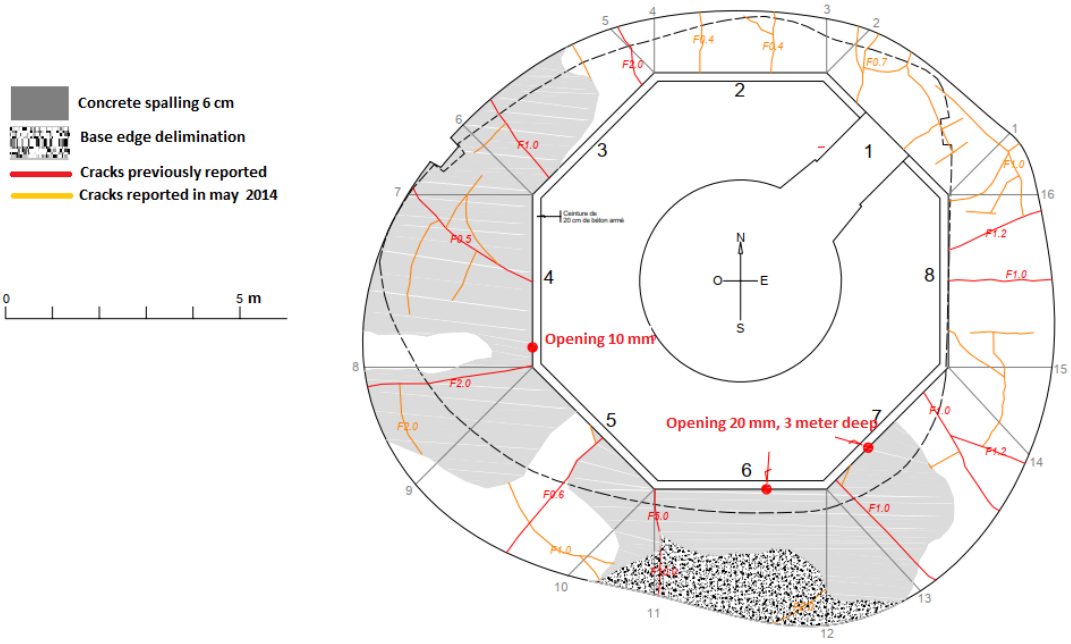

Figure 46:Planer view of the condition of the base after the inspection of May 2014 by CEREMA St Brieuc [34].

A series of extreme storms in 2014 damaged around 50% of the platform surface which was later covered by dry mix shotcrete in 2015 as shown in figure 47.

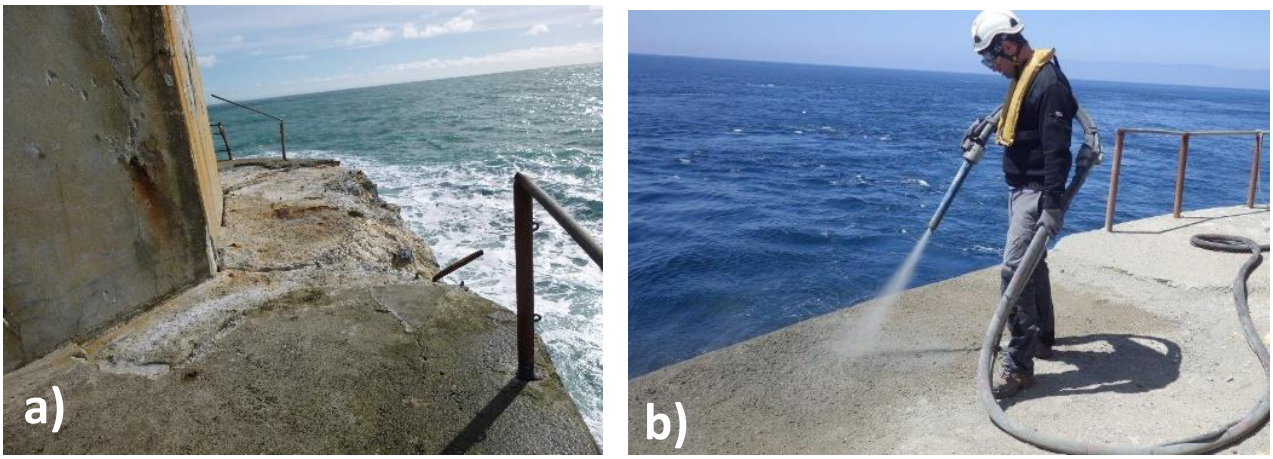

Figure 47: Base Platform: a) Spalling and radial cracks [32]; b) Shotcrete application [33]

8.3 Protection and reinforcement interventions

8.3.1 Challenges and Context

The main challenge for reinforcement intervention for offshore structures is the limited access time (few days a year) due to weather conditions as well as tidal level and tide coefficients. The intervention work is recommended to be performed in calm weather with high tide coefficient at the time of low tidal level. A high tide coefficient (spring tide) means a very low tidal level twice a day and a very high tidal level twice a day.

Thin layers of **U**ltra-**H**igh-Performance **F**iber-**R**einforced **C**oncrete ''UHPFRC'' have been applied in many existing structures such as bridges and buildings over the last 18 years [35].

UHPFRC are considered very suitable for the reinforcement of Maritime structures due to their extreme low permeability, their outstanding mechanical properties with a robust tensile Strain Hardening, their durability, and their cost efficiency on the long run [36].

The first application of UHPFRC with steel fibers on an existing maritime structure in France, was on a turret in the bay of Lorient in Brittany in 2013 in collaboration between MCS/EPFL and CEREMA. 60 mm layer was cast in place using a helicopter to reinforce this existing turret [35]. Moreover, the application of synthetic fiber based UHP-SHCC for the reinforcement of piers in harbor sites was investigated and validated by [38].

Consequently, the application of targeted reinforcement of UHPFRC is optimal for structures in the marine environment such as signalization structures (turrets and lighthouses) exposed to the most severe environment conditions.

The aim of this section is to propose a solution to protect the base of La Jument using UHPFRC as well as to highlight the importance and the main characteristics of PE- UHPFRC.

8.3.2 PE- UHPFRC Characteristics

The fibers used are made of Ultra-high-molecular-weight Polyethylene UHMW-PE to replace the steel fibers. These new low clinker strain hardening mixes have proven to reduce environmental impact with outstanding potential durability [37].

UHPFRC with steel fibers is a cementitious material with a much higher compressive strength ≅ 200 MPa than normal concrete, a tensile strength of 8 to 18 MPa, and a strain hardening domain of 1‰–2‰.

PE- UHPFRC are an improved version of the UHPFRC with steel fibers. Their outstanding mechanical properties and their role in reducing environmental impact were demonstrated by [37]. Furthermore, PE-UHPFRC have excellent synergies with steel rebar, due to their very large deformation at the end of hardening

The hardening capacity for UHPFRC with synthetic fibers 35‰ is 10 to 20 times larger than that of steel fibers UHPFRC whereas their softening behavior is less. The length of PE fiber is 6mm, less than the steel fiber which is typically 10 to 15 mm, but with a much smaller diameter of 12 microns vs 0.175 to 0.2 mm for steel fibers.

The maximum crack width is expressed in equation 14.

$$w_{max} = \frac{L_F}{2}$$ *Equation 14 where L_F is the fiber length.*

Table 9 summarizes the main characteristics of UHPFRC with steel fiber as well as with PE fibers and figure 48 illustrates the tensile response of both type of UHPFRC.

Table 9: Typical UHPFRC mechanical properties (steel fibers vs synthetic fibers) [37] fute =Tensile Elastic limit; futu = Tensile strength; ε_e =elastic strain; ε_u =Ultimate strain

	Steel- UHPFRC	**PE- UHPFRC**
E [MPa]	51000	42600
Compressive strength [MPa]	230	120
f_{ute} [MPa]	10	7.7
f_{utu}[MPa]	13	11.7
ε_e [mm/mm]	0.19 ‰	0.18‰
ε_u [mm/mm]	2 ‰	35‰

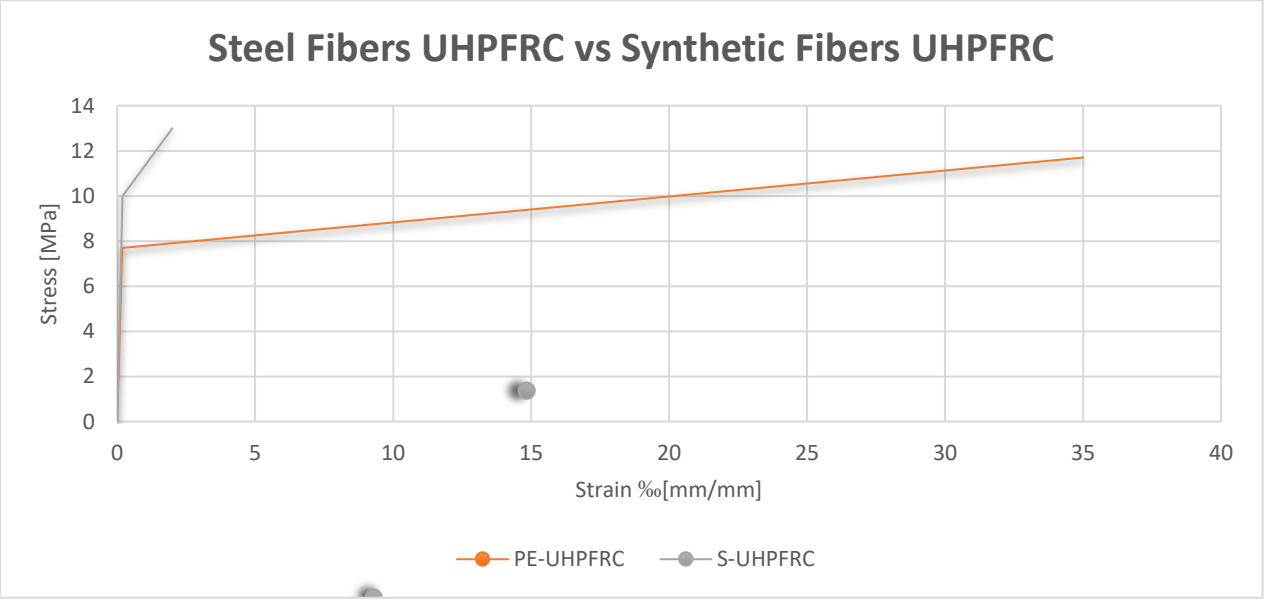

Figure 48: Steel-UHPFRC vs PE-UHPFRC [33]

8.3.3 Concept of reinforcement with PE-UHPFRC

Structural enhancement of the base of La Jument is at most importance based on its current state. The main purpose is preventing water penetration in order to minimize their effect in widening the existing radial cracks as well as to protect against any possible chloride attack.

There are two scenarios presented in figure 49.

The first is proposed in this study to prevent water infiltration in the base of the tower, illustrated in figures 49 a and 50.

Applying *a 60 mm layer is recommended to reinforce the upper level of the base '' the platform'' in which many radial cracks and concrete spalling was found. This must be implemented after demolition of the old damaged platform. It must be anchored with base. The volume of UHPFRC needed is approximately 4.5 m^3. A workability maintained 2 to 3 hours is recommended [35].*

In addition to the large deformation capacity of the PE-UHPFRC, they have many advantages over Steel UHPFRC for the scope of this study. It has 10 times less dead weight per cubic meter as well as no rust surface will be formed on the top of the platform in the long run. Furthermore, PE-UHPFRC have an excellent protective function with extremely low water and gas permeability which is the characteristic needed in this proposal.

The second scenario discussed by [4] is to reinforce the concrete ring around the base of the tower which is heavily damaged as well as confining part of the top base and the platform, figure 49 b. This would add stiffness to the tower which might create restriction against vibrations and then generates higher stress and cracks in the masonry. One of the main limitations also is the size and the amount of formwork needed to be applied around the base with an approximately 13 meters diameter. Thus, it is challenging, but feasible with sprayed UHPFRC for example.

Limitation of vibrations is not as important as protecting the base. Confining the base and the tower by UHPFRC adds stiffness to the structure and restrict oscillations. This induces higher stresses in the masonry due to extreme waves actions and causes cracks.

The main essential reinforcement against enormous vibrations mentioned by the archives was the second enlargement of the base to resist storms waves. This was confirmed by FEM calculations.

Therefore, protecting the base by a durable material with high deformability is the main objective to confine the radial cracks and to prevent water infiltration. The opening must be closed with a non-stiff material such as foam material. Letting the tower oscillating in the 20 mm opening gives more flexibility for the lighthouse. Thus, the second scenario which is connecting the base and the tower is not recommended.

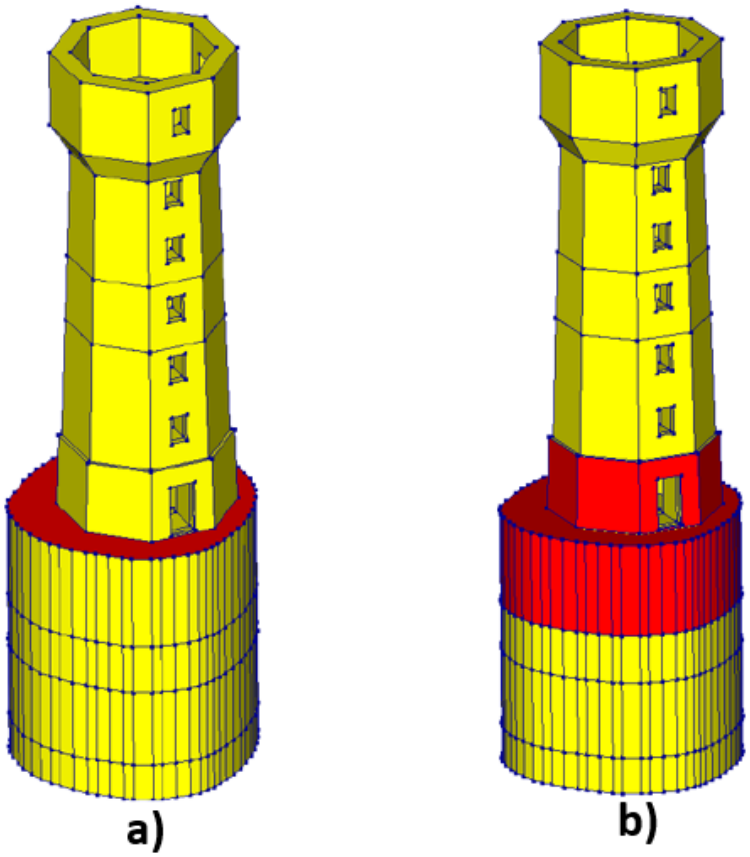

Figure 49: UHPFRC Zone of applications; a) Scenario proposed; b: Scenario previously proposed by [4]

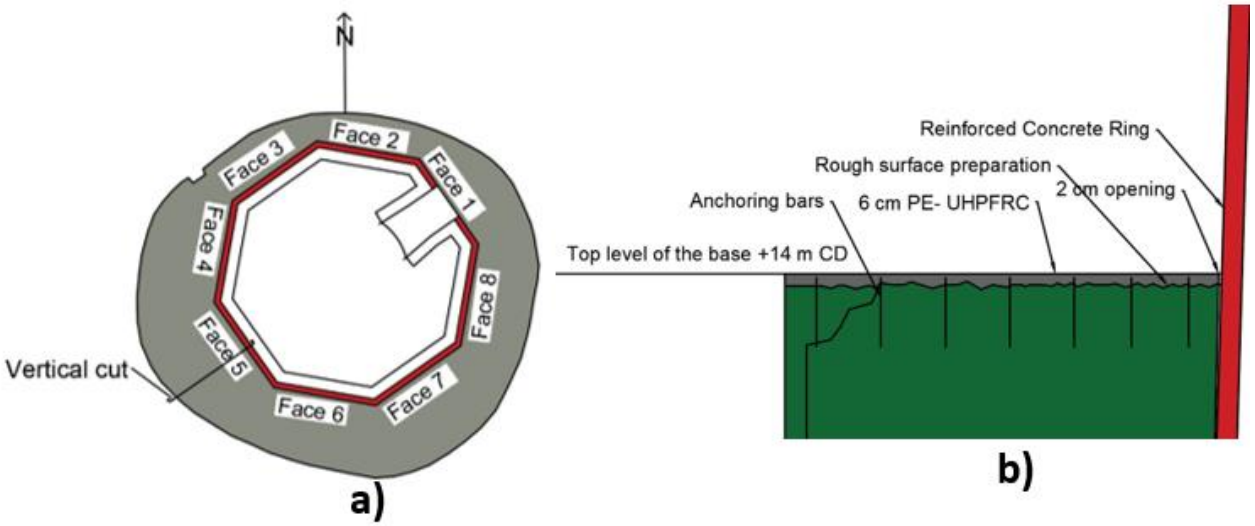

Figure 50: PE- UHPFRC reinforcement: a) top view, b) vertical section

8.4 Measurements campaign and monitoring

8.4.1 Literature and motivation

In-situ waves load measurements are essential to know the exact impact area with the relative pressure magnitude. Many experimental studies are conducted in 2D setup with scaling prototypes whereas the ‘’nonlinear ‘’ wave breaking is a 3D phenomenon, and therefore, this could lead to underestimation of the maximum pressure. The first attempt to measure wave impact in the field was in 1938 by [40] using (quartz piezoelectric sensors of 6 cm diameter). The pressure measured in this experiment was between 180 and 690 kPa which is the largest value ever recorded in situ. Other experiment was implemented in 1989 at Alderley breakwater with an impact value of 396 kPa [41]. Recently, a 4 month in-situ wave impact pressure measurements campaign was implemented using KELLER sensors at the Artha-dyke [39] in the south-west of France.

In the Ushant island, the average tide level for 100 years return period is around 4.6 m [7-25] and for the significant height is about 14.7m [3-42]. Thus, a giant rogue as high as 29.4 m could happen. Pressure transducers must be integrated in the most likely area to be impacted by the largest waves’ impulse. This area can be identified by means of photographic documentation, visual observation of damages, stereo video registration. To maximize the benefits of this campaign, the installment must be combined with accelerometer data and oceanographic statistics such as weather conditions, tidal level, waves direction and waves significant height.

8.4.2 Measurements period

Many remarkable events have happened at the Ushant island. Numerous observations for different storms occurred in 1990 and 2011 confirmed that most of the remarkable storms occurs between December and March [42]. Recently, a 24.6 m wave was observed in February 2021. Thus, the measurement campaign is recommended between January and February.

8.4.3 Pressure transducers specifications

The sensors must be able to give reliable data measurements in extreme weather conditions. The range of pressure must be between 0 and 10 bar preferably 0 and 5 bar since the estimated slamming pressure is between 0 and 500 kPa equivalent to 5 bar. High pressure range (0-50 bar) can lack of accuracy in recording low impact pressures.

In figure 52, a piezo-resistive sensor PAA25 by Killer is illustrated. It mainly quantifies the force by measuring the corresponding change in electrical resistance. After contacting Keller, this transducer is an absolute pressure transmitter. It must be combined with photovoltaic system due to the absence of electricity. Its response time is less than 5 milliseconds which good for the impulsive loading period considered in this study 50 milliseconds. The normal frequency of the sensor is 1kHz and its lifetime is 10 million cycle.
The advantage of these sensors is that one can remotely have access to the data. The data must be analyzed with an effective processing procedure.

8.4.4 Pressure transducers Proposition

More sensors are proposed on the octagonal tower than the substructure since there are more uncertainties about the horizontal distribution of waves loading. It seems that the adjacent faces of face 5 can grip more pressure than cylindrical tower. Moreover, the main aim is to measure the slamming impact of the extreme breaking waves. They are most likely to be hitting the tower and not the base. High loading on the substructure does not cause notable acceleration and displacement according to FE calculation [4]. This is confirmed by one simulation in DIANA 10.5.

As for the horizontal distribution, the focus mainly on face 4 and 5 since. The most likely direction of waves is hitting the corner of face 4 and 5 taking into consideration that the swell might change its direction in the last 50 meters before the lighthouse due to the sudden increase in the rock formation.

24 sensors are proposed to be installed on the tower and 8 on the substructure. Their distribution is presented in figure 54. There are 5 pressure transducers PAA 25 Keller already integrated at 5 different positions on la Jument external faces. Two of them are integrated on face 5 in 2 different position and are illustrated in figure 53. The location of each transducer is presented in table 10. Unfortunately, the data collected is not yet analyzed.

Table 10:Pressure Transducer Location at La Jument (Already integrated)

Sensors ID	Location	Height with reference to CD (m)
P1	External Masonry (Face 5)	+20.0
P2	Reinforced Concrete Ring (Face 5)	+17.0
P3	Substructure (Below Face 5)	+13.0
P4	Reinforced Concrete Ring (Face 4)	+17.0
P5	Reinforced Concrete Ring (Face 6)	+17.0

Figure 51:KELLER Pressure Transducer PAA 25[47]

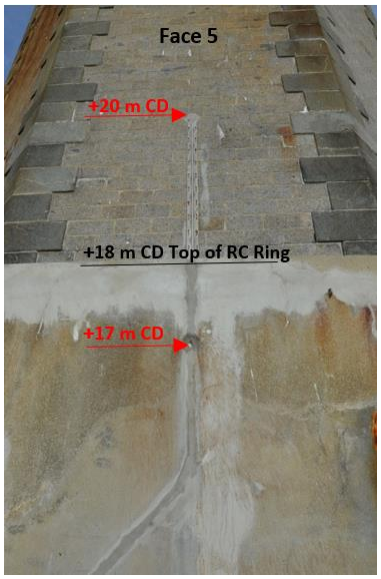

Figure 52:Pressure Transducers at face 5 +17.0 m and +20 m CD

According to Keller, each sensor can cost approximately 500 CHF. However, according to Mr. Fady - CEREMA, the sensors already integrated in la Jument costed approximately 2000 € per sensor including the cost of shipment and installation. Thus, the total cost estimated is around ((32-5)× 2000) = 54000 €.

The pressure transducers already integrated are represented by green circles whereas the pressure transducer proposed are represented by red circles. They are illustrated in figure 54.

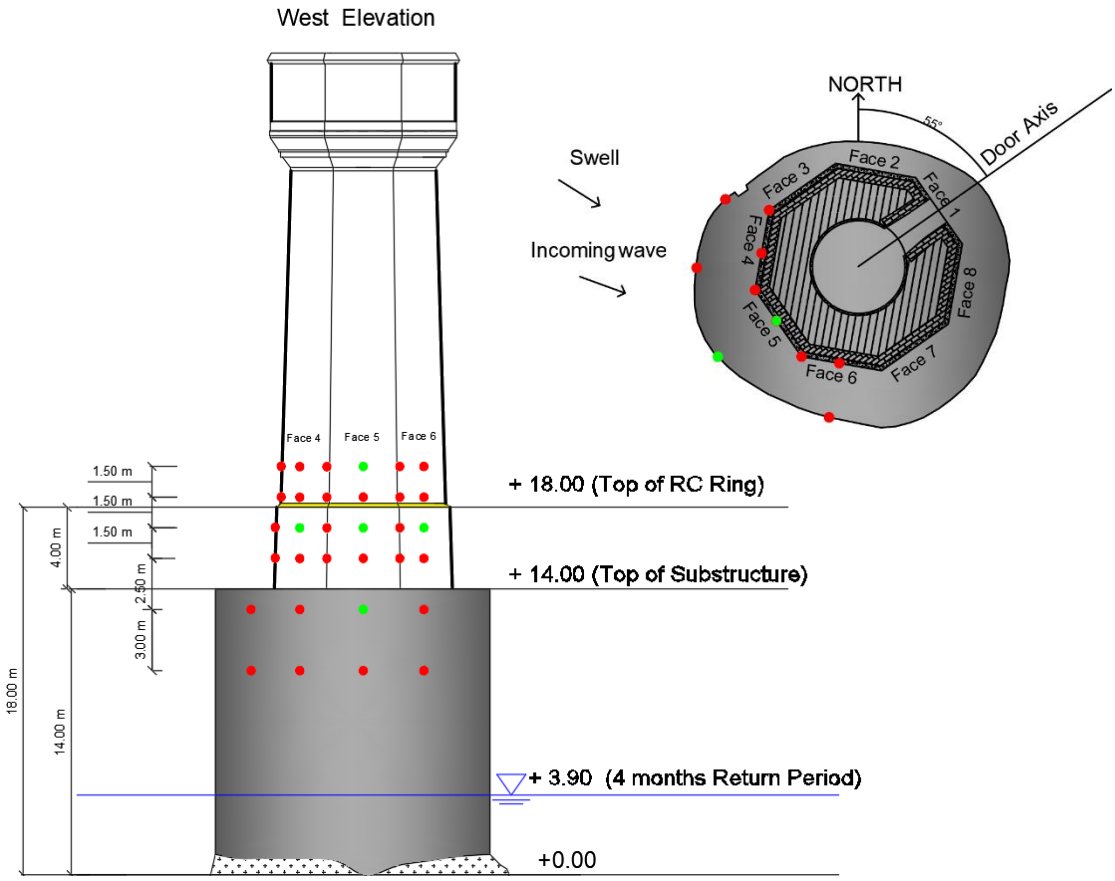

Figure 53: Vertical and Horizontal pressure transducers distribution (Green: Installed, Red: Proposed)

The proposal will help in understanding waves characteristics and in confirming the hypothesis related to La Jument as well as in better calibrating the FE model. It helps surely in removing the uncertainty about the pressure magnitude, the loading time, and the vertical and horizontal distribution of loads. The priority for pressure transducer integration goes for the ones of the octagonal tower and not for the substructure. The variation of pressure as function of the waves' characteristics (Hs, Tide level, period, speed) can be analyzed as well by "lm" routine from R software as in [39]. Time-pressure history, which is major results of this campaign, will help significantly in future FEM calibrations.

8.5 Modulus of Elasticity Estimation

In-situ measurement must be performed on La Jument lighthouse to remove the ambiguity about the cracked modulus of elasticity. Non-destructive methods are more preferred than destructive methods such as core drilling which can be used to get the compressive and tensile response as well as the modulus of elasticity. Furthermore, Non-destructive method can be used to assess the geometrical shape and state of the lighthouse such as cavities, cracks, heterogeneity in layers, texture, and thickness.

The ultrasonic pulse velocity (UPV) approach [43] is one of the most widely utilized non-destructive methods to assess the quality of concrete, as well as the location and depth of cracks in both reinforced and masonry structures. The values of dynamic elastic modulus of concrete can be estimated using this method. Other methods based on LIDAR Scanning can be utilized. LIDAR stands for Light Detection and Ranging can provide high precision for distances, textures, thickness and other. It works as 3 D points cloud technique and is already implemented for historical building maintenance [44].

The UPV and LIDAR are recommended for the octagonal tower to get a clear idea about the existing cracks as well as to get an indication about the dynamic modulus of elasticity. It can be used as well for the basement.

A ground-penetrating radar (GPR) can be used to locate reinforcing bars, detect rebar corrosion, estimate the rebar size, evaluate the concrete cover, and assess the concrete characteristics (i.e uniformity, voids, cracks, strength and durability) by examining the material dielectric properties. The interpretation of the back-reflected signal provides an evaluation of the properties and the geometry of the subsurface [45].

Thus, *the GPR is highly recommended to assess the state of the reinforced concrete ring as well as to the tower-base and base- rock connections.*

9 Conclusions and future work

The structural response of La Jument lighthouse under extreme waves loading is characterized through finite element calculations using DIANA 10.5 software. The model was defined and improved based on the structural dimensions and materials from the archives, on the basis of previous works form Loraux [4].

The wave considered for this study is the highest wave measured during a monitoring campaign in January 2018 which was essential to assess the dynamic response of the lighthouse under waves actions. The modulus of elasticity and damping characteristics used in the FE model were calibrated based on the spectral analysis of the in-situ accelerations measurements [3]. Photographical documentations were crucial as well to check the accuracy of the model.

This parametric study demonstrated the effect of the tide level, the slamming pressure magnitude, and the slamming area on the structural response of the lighthouse. The main results obtained are:

1. The FE model suggested a 230 kPa as the most likely pressure of the wave under consideration. This pressure is actually close to values calculated by [21]. The wave considered in [21] was a 20-meter wave with an 11 seconds period whereas wave 1 considered in this study was a 19-meter wave with a 13 seconds period.
2. A global modulus of elasticity of 15 GPa represents the actual cracked state of La Jument lighthouse. The natural frequencies calculated by DIANA with 15 GPa modulus of elasticity were the closest to the ambient vibration analysis in calm weather [29] and the spectral response analysis of accelerometers measurement [3].
3. The tide level was proven to be an important factor contributing to the increase in structural responses parameters. The displacement and acceleration can increase up to 50% approximately going from a low tide level to the maximum tide level +8.2 m CD at La Jument. [7] confirmed the influence of tide levels on the structural response of the Eddystone lighthouse.
4. The FE model was able to predict the accelerations measurements accurately. The accelerations obtained from FEM calculations were similar to the ones extracted from the accelerometers. This similarity gives confidence to the FE model as well as to the hypothesis implemented in this project [11].
5. The displacement calculated by FEM were higher than the actual displacement obtained by double integration of the measured accelerations. This discrepancy results from the assumed direction of the wave under analysis which can be optimized in future simulation to get closer to the real measurement.

Several improvements are recommended as well such as modeling the cracks separating the tower and the base as an interface in FE software and trying a better method of numerical integration to calculate the displacement since the values calculated by DIANA seems to be overestimated.

The upper level of the base, the platform, must be reinforced by UHPFRC layer to prevent water infiltration from existing cracks which helps in extending the serviceability life and maintaining the safety of La Jument lighthouse. The layer is recommended to be anchored in the basement with a thickness of 6 cm. The volume of UHPFRC needed is approximately 4.5 m^3. Not connecting the tower and the base is recommended as well to keep the tower flexible. UHPFRC workability must be maintained over 2 to 3 hours. The separation between the tower and the basement must be closed by foam.

Carrying a measurement campaign for waves pressure is proposed to remove the uncertainty about the pressure magnitude, the loading time, and the vertical and horizontal distribution of loads. This helps in better calibration of the FE model for future calculations and in confirming the hypothesis related to waves to provide better estimation for their actions. Most of the hypothesis are based on cylinders under waves actions whereas La Jument has an octagonal tower and an imperfect cylindrical base. Thus, this would be an opportunity to study the horizontal distribution waves for such shapes and to confirm assumption taken in this study which is octagonal shapes gives more grip to the applied waves actions than cylindrical shapes.

The proposed measurement campaign paves the wave to estimate the pressure-time history of the waves hitting the lighthouse. This is one of the most important parameters to calibrate in future studies. It can be used in future simulations to better understand the effect of waves action on the structural response as well as to assess the structural health of the lighthouse for any future intervention.

10 References

1. Direction Interrégionale de la Mer Nord Atlantique Manche Ouest. (2017). *Phare de la Jument. Phare de la Jument* - Direction Interrégionale de la Mer Nord Atlantique Manche Ouest. Available from: http://www.dirm.nord-atlantique-manche-ouest.developpement-durable.gouv.fr/phare-de-la-jument-a85.html?debut_portfolio=12#pagination_portfolio
2. Filipot J-F, et al. (2019) " La Jument Lighthouse: a real scale laboratory for the study of giant waves and of their loading on marine structures " , Phil Trans R Soc A.
3. Denarié E., Fady N., (2019), "Structural response of French offshore heritage lighthouse, Phil. Trans. R. Soc. A., doi: 10.1098/rsta.2019.0011, Volume 377, Issue 2155, Article nu mber 20190011
4. Loraux C. (2013), '' Comportement structural des phares en mer, étude historique sur le phare de la Jument et propositions d'interventions'', Master thesis. Lausanne: EPFL;
5. Chollet O. Phare d'Ar-Men, Modélisation des effets de la houle, analyse du comportement structural et études de renforcement. Master thesis. Lausanne: EPFL; 2014.
6. Pappas, Athanasios & D'Ayala, Dina & Dassanayake, Darshana & Antonini, Alessandro & Raby, Alison. (2021). Rocking of offshore lighthouses under extreme wave impacts: Limit analysis, analytic formulations and distinct element method. Engineering Structures. 228. 10.1016/j.engstruct.2020.111534.
7. Trinh, Quang & Raby, Alison & Banfi, Davide & Corrado, Mauro & Chiaia, Bernardino & Rafiq, Yaqub & Cali, Federico. (2016). Modelling the Eddystone Lighthouse response to wave loading. Engineering Structures. 125. 566-578. 10.1016/j.engstruct.2016.06.027.
8. Morison, J., O'Brien, M., Johnson, J., & Schaaf, S. (1950). The forces exerted by surface waves on piles. Journal of Petroleum Technology, Petroleum Transactions, AIME 189, 149-154.
9. Zhou D., Chan E.S., Melville W.K., (1991), "Wave impact pressures on vertical cylinders", Applied Ocean Research, Vol. 13, N° 5
10. Goda Y, Haranaka S, Kitahata M. Study on impulsive breaking wave forces on piles. Port and HarbourTechnical Research Institute; 1966.
11. Wienke J, Oumeraci H. Breaking wave impact force on a vertical and inclined slender pile - Theoretical and large-scale model investigations. Coast Eng 2005;52: 435–62. https://doi.org/10.1016/j.coastaleng.2004.12.008.
12. Perlin M, Choi W, Tian Z. 2013 Breaking waves in deep and intermediate waters. Annu. Rev. Fluid Mech. 45, 115–145. doi:10.1146/annurev-fluid-011212-140721
13. Blenkinsopp CE, Chaplin JR. 2011 Void fraction measurements and scale effects in breaking waves in freshwater and seawater. Coastal Eng. 58, 417–428. doi:10.1016/j.coastaleng.2010.12.006
14. Miche A. 1944 Mouvements ondulatoires de la mer en profondeur croissante ou décroissante. forme limite de la houle lors de son déferlement. application aux digues

maritimes. Troisième partie. Forme et propriétés des houles limites lors du déferlement. Croissance des vitesses vers la rive. Ann. Ponts et Chaussées Tome 114, 369–406.
15. Wienke, J., U. Sparboom and H. Oumeraci. 2000. Breaking wave impact on a slender cylinder, Proc. of the 27th ICCE, Sydney.
16. Oumeraci H., Klammer P., Partenscky H.W. (1993) Classification of breaking wave impact loads on vertical structures, ASCE, J. Waterway, Port, Coastal and Ocean Eng., 119(4), 381-397
17. Haver, S. 2004 A possible freak wave event measured at the Draupner jacket January 1 1995. In Rogue waves Workshop, Brest.
18. Haver, S. (2004). ''Freak Waves: A Suggested Definition and Possible Consequences for Marine Structures''
19. Von Karman T. The impact on seaplane floats during landing. NACA technical notes. 1929; (N° 321).
20. Faulkner, Douglas (2000). Rogue Waves – Defining Their Characteristics for Marine Design (PDF). Rogue Waves 2000 Workshop. Brest: French Research Institute for Exploitation of the Sea. p. 16.
21. Huo, F.; Yang, H.; Yao, Z.; An, K.; Xu, S. Study on Slamming Pressure Characteristics of Platform under Freak Wave. J. Mar. Sci. Eng. 2021, 9, 1266. https://doi.org/ 10.3390/jmse9111266
22. Myrhaug, D., and S. P. Kjeldsen (1986), Steepness and asymmetry of extreme waves and the highest waves in deep-water, Ocean Eng., 13, 549 – 568.
23. Alain Cavanie, « La houle déferlante et son action », Conférence présentée au cours du VIème Colloque de l'ASTEO - Centre Océanologique de Bretagne, 14-15-16 février 1974, p. 1
24. Lundgren, H. (1969, March). Wave shock forces: an analysis on deformations and wave forces in the wave and the foundation. In Symposium" Research on wave action", Delft, The Netherlands, March 24-26, 1969.
25. Courtesy, "Jean-Denis le Pape (2022), Sonar measurements around La Jument Ligfhthouse, Armement FInisterrae".
26. Ardhuin F. Position de la surface de la mer par rapport au niveau moyen - du goulet de Brest à Portsall, île d'Ouessant: IFREMER; 2022; available from: https://marc.ifremer.fr/resultats/niveaux/modeles_mars2d_atlantique_nord_est/(typevisu)/map/(zoneid)/7066#appTop
27. Hordijk DA. Local approach to fatigue of concrete. Doctoral thesis: TU Delft; 1993.
28. Scotta, R., Vitaliani, R., Saetta, A., Oñate, E., & Hanganu, A. (2001). A scalar damage model with a shear retention factor for the analysis of reinforced concrete structures: theory and validation. In Computers & Structures (Vol. 79, Issue 7, pp. 737–755). Elsevier BV. https://doi.org/10.1016/s0045-7949(00)00178-4
29. Loraux C. Campagne de mesure sur les phares de la Jument et du Creach, mesure des vibrations ambiantes et relevé de l'état (Jument seulement). EPFL; 2013. Report no. MCS 23.13.09-1

30. Lestuzzi, Pierino. (2002). Effective Stiffness of RC Walls in Dynamic Tests.
31. Chopra, Anil. (2007). Dynamics of Structures – Theory and Applications to Earthquake Engineering.
32. Denarié E., Visual Inspection, Pictures taken in Ushant 2014
33. Fady N., La Jument supervision work, Pictures taken in Ushant 2015
34. Benoit Thauvin, Patrick Le Roy (2014), “Rapport de l'inspection du soubassement du phare de la Jument (phase 1)”, CEREMA St Brieuc
35. Denarié E., (2018), ‘’UHPFRC for the cast in place reinforcement of offshore maritime signalization structures’’, Invited lecture for HAC2018 | V Congreso Iberoamericano de Hormigón Autocompactante y Hormigones Especiales, Valencia, 5 y 6 de Marzo de 2018, Eds Aitor Llano Torre, José Rocio Marti-Vargas, Pedro Serna Ros, Editorial UPV, 17-30
36. Hajiesmaeili, Amir & Hafiz, M. & Denarié, E.. (2021). Tensile response of Ultra High Performance PE Fiber Reinforced Concretes (PE-UHPFRC) under imposed shrinkage deformations. Materials and Structures. 54. 114. 10.1617/s11527-021-01621-0.
37. Hajiesmaeili, Amir & Denarié, Emmanuel. (2018). Next Generation UHPFRC for Sustainable Structural Applications. Aci Materials Journal. 326. 58.1-58.10.
38. Tanaka R., Kunieda M., Iwanami M., Kato E., Amino T. (2016), "Jacketing Method for Pier Piles using UHP-SHCC", Proceedings BEFIB 2016, Vancouver, 406-4
39. Larroque, Benoit & Arnould, P & Luthon, Franck & Poncet, Pierre-Antoine & Rahali, A & Abadie, Stéphane. (2018). In-situ Measurements of Wave Impact Pressure on a Composite Breakwater: Preliminary Results. Journal of Coastal Research. 85. 10.2112/SI85-218.1.]
40. A. de Rouville, P. Besson, and P. Petry. Etat actuel des études internationales sur les efforts dus aux lames. 1938. Google-Books-ID: _SDCoAEACAAJ.
41. Bullock, G.N., Crawford, A.R., Hewson, P.J., Walkden, M.J.A.,and Bird, P.A.D, 2001. The influence of air and scale on wave impact pressures. Coastal Engineering, 42(4):291–312
42. CEREMA– Fiches synthétiquess des mésure des étas de mer du réseau CANDHIS (2021) ; available from: https://www.cerema.fr/fr/centre-ressources/boutique/fiches-synthetiques-mesure-etats-mer-maj-2021
43. Mohammad, Iqbal Khan. "Non-destructive testing for concrete: dynamic modulus and ultrasonic velocity measurements." Advanced Materials Research. Vol. 243. Trans Tech Publications Ltd, 2011.
44. Nasrollahi, M., N. Bolourian, and A. Hammad. "Concrete surface defect detection using deep neural network based on lidar scanning." Proceedings of the CSCE Annual Conference, Laval, Greater Montreal, QC, Canada. 2019.
45. Tosti, F., & Ferrante, C. (2020). Using ground penetrating radar methods to investigate reinforced concrete structures. Surveys in Geophysics, 41(3), 485-530.
46. DIANA (2021) , DIANA user’s manual, Release 10.5
47. Keller AG. (n.d.). Retrieved January 27, 2022, from https://keller-druck.com/fr

Appendixes

Appendix 1: Accelerometers Location

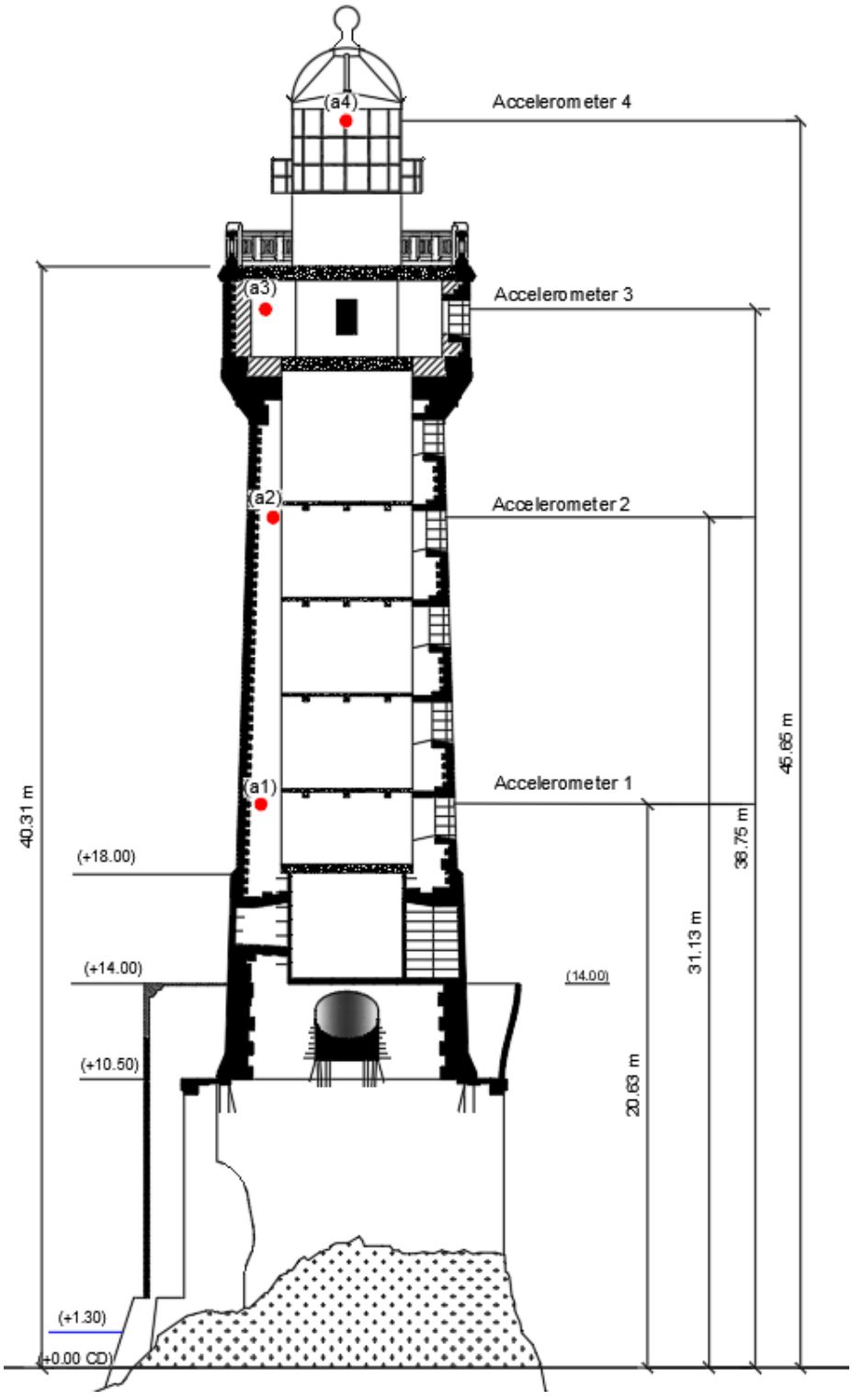

Figure 54: Accelerometers Location in measurements Campaign (2018)

Appendix 2: Return period of Hs, Tide level, and Storm surge

Significant height and average tide level return periods are extracted from ‘’Fiches synthétiques de mesure des états de mer du réseau CANDHIS Tome 1 - Mer du Nord, Manche et Atlantique ‘’ - by CEREMA for the Ushant Island.

Storm surge return periods are extracted from ‘’ Les niveaux Marins extrême Ports de métropole ‘’ by CEREMA for the the ‘Conquet ‘ Island which is the closest to Ushant island

Table 11: Return period of Hs, Tide level, and Storm surge

Return period (Years)	Significant height (m)	Average Tide level (m)	Storm surge (m)
5	10.8	4.28	0.73
10	11.8	4.34	0.8
20	12.7	4.42	0.87
50	13.9	4.51	0.95
100	14.7	4.57	1.02

Appendix 3: Master's Project Schedule (Gant Chart)

The project duration is 17 weeks starting from 27th September 2021 and ending in 28th January 2022. The thesis will be defended in the 17th of February 2022.